J. Fluid Mech. (1980), *vol.* 98, *part* 1, *pp.* 1–31
Printed in Great Britain

A modelling of large eddies in an axisymmetric jet

By E. ACTON

Engineering Department, University of Cambridge†

(Received 19 August 1977 and in revised form 6 March 1979)

Crow & Champagne (1971), Bechert & Pfizenmaier (1975) and Moore (1977) have observed that the growth, mixing and noise production of jet flows are sensitive to harmonic forcing. This paper describes an attempt to model numerically certain features of these flows. The model flow is restricted to be axisymmetric and is consequently unrepresentative of the detailed structure in a real jet. Nonetheless, it is found that reasonable qualitative agreement exists between the results of the model and experiments as far as the large eddies are concerned. This suggests that a substantial part of the large-scale structure in a jet is essentially axisymmetric. Harmonic excitation is also applied to the model jet and the changes in frequency and amplitude of the excitation cause distinct changes in the wavelengths of the jet eddies. This resulting large-eddy behaviour is consistent with many features of the nonlinear behaviour observed experimentally in forced jets.

1. Introduction

Flow visualization techniques have revealed a large-scale structure in turbulent shear flows. In their experiments on subsonic turbulent jets, Crow & Champagne (1971) showed that the large-eddy structure and the growth and mixing of the jet were sensitive to harmonic forcing. They suggested that the large-scale development of the jet up to an axial distance of five diameters could be completely controlled by slight exit plane forcing. Crow & Champagne found a 'preferred' frequency for the development of the jet which, non-dimensionalized by the jet diameter and exit velocity, was a Strouhal number $St = 0{\cdot}3$. They believed that this frequency was 'preferred' because the wave attained the highest possible amplification under the combined effects of linear amplification and nonlinear saturation.

Chan (1974) measured the spatial development of pressure waves in a round turbulent jet (Reynolds number $Re = 2{\cdot}6 \times 10^5$) subject to internal acoustic excitation. The pressure disturbances grew to a maximum some distance from the nozzle exit and then decayed. The most amplified mode was at $St = 0{\cdot}5$ in the shear layer and at $St = 0{\cdot}35$ on the jet axis. Bechert & Pfizenmaier (1975) excited internally a subsonic jet with harmonic plane acoustic waves. They discovered an altogether new and unexpected phenomenon: there was an associated amplification of broadband jet noise. The frequency of the forcing was $St = 0{\cdot}5$, and the ratio of the r.m.s. value of the exit velocity fluctuations to the mean velocity at the nozzle exit was 0·0038. The radiated sound was caused by the acoustic excitation but did not differ much in angular and spectral distribution from the unforced jet noise. Lip noise and flow separation were shown to be irrelevant to the effect.

† Present address: Topexpress Ltd., 1 Portugal Place, Cambridge CB5 8AF.

0022–1120/80/4521–1370 $02.00

The increase of the broadband noise generation of a forced jet was discovered independently and concurrently by Moore (1977). A turbulent jet ($Re = 3 \times 10^5$) with a fairly thick turbulent boundary layer was excited internally with acoustic plane waves. Above a certain level of forcing, the response of the jet was nonlinear and the broadband pressure fluctuations, both inside the jet and in the far field, were affected. Below a Mach number $M = 0{\cdot}7$, the behaviour was only weakly dependent on Mach number and all jets showed a peak increase in broadband noise when forced with $St = 0{\cdot}35$. As the Strouhal number was increased, this increase in broadband noise lessened until there was a resulting decrease in broadband noise for $St > 1{\cdot}5$. Moore also visualized the flow for $St < 1$ and observed that at forcing levels at which the response of the jet was nonlinear, there was a dramatic 'locking-on' of the large eddies to the excitation frequency.

It is thus clear that the large eddies in turbulent jets and their effect in the far field can be controlled by harmonic forcing. It is apparent from the pictures of Moore that the forcing was changing the eddy wavelengths, and also that a substantial part of the large-eddy structure is axisymmetric. It is therefore of interest to attempt to model this large-eddy development in a turbulent jet and investigate the effect of harmonic forcing. Following our previous study of similar flows (Acton 1976), we attempt here such a modelling and represent the jet shear layer by discrete vortex elements and consider an axisymmetric jet developing from rest. Ring vortex elements are used to represent the jet shear layer and its computed development into large eddies is investigated with and without forcing. Such a modelling of a jet flow by discrete vortex elements is not new. Davies & Hardin (1973) successfully modelled a starting jet in that way. The use of the model to visualize the effect of harmonic forcing on the large-scale structures is new and represents a natural extension of the earlier work.

We are now attempting to model a developing axisymmetric jet and therefore some representation of the nozzle flow is necessary. We do not satisfy the boundary conditions exactly; we define a parallel flow in the jet pipe and represent it by ring vortex elements. This is an approximation of the effect of the jet pipe on the jet shear layer and diffraction at the nozzle edge is not modelled at all. As in our previous study, the smallest scales of the motion in the shear layer are not modelled; a smoothing core is applied to each ring element neighbouring elements, and avoids the need to evaluate these apparently active small-scale motions.

This axisymmetric-jet model is that of inviscid flow. We found that the absence of viscosity was unimportant in our previous model but in this case we shall have as a consequence areas of potential flow in regions where they are known to be impossible. For example, the entrainment of irrotational fluid is we think represented realistically but in our model the entrained fluid remains unrealistically irrotational because the viscous diffusion of vorticity over small scales is excluded. In many areas of the model flow, although the vortex elements are widely distributed, the flow outside them remains potential. This is not turbulence but may easily be thought of as part of the large eddy motion which is known to be essentially inviscid (Townsend 1976). Therefore, because in our model the smallest scales of motion are smoothed out, we can only be concerned with the large-scale motion; it is the large eddies which have been shown to be so significant in experiments that we are attempting to simulate. Thus, in our computations, we expect not to look closely at the motion of individual elements but to take a global view of the jet development in terms of the larger eddies. The effect of

forcing on the large-eddy development can thereby be modelled and from that modelling we hope to provide some interpretation of the features observed experimentally in forced jets.

The results of our jet model are described in § 3 and § 4. As in our earlier study, concentrations of vorticity evolve in the shear layer, and are seen to interact by rolling around one another and coalescing. However, the location and frequency of this occurrence now depends on the relative size and spacing of the eddies in the shear layer, which are greatly altered by the forcing. Despite the model's obvious and several shortcomings, the computed unforced jet flow is similar to those observed experimentally. The mean flow development, shown in figure 7, compares well with that observed experimentally in the mixing region and the initial entrainment rate for this inviscid jet model is also in reasonable agreement with that observed experimentally as shown in figure 16. The forced model jets also show features observed in the experiments. These forced jets were computed for a necessarily short time; the jet upstream of the starting vortex was allowed to develop for an axial distance of approximately six diameters. This is just sufficient to observe the changes in eddy development in the mixing region; the computation was taken no further because of the large demand on computer time.

We show for these forced model jet flows that, in the Strouhal number range $0{\cdot}3 \leqslant St \leqslant 2{\cdot}0$, forcing of sufficient amplitude can excite the jet eddies at the forcing wavelength. When $St = 0{\cdot}3$, these eddies are very large and form at $X/D \simeq 2{\cdot}0$. When the jet is forced at $St = 0{\cdot}5$, the large eddies form at $X/D \simeq 1{\cdot}0$ and persist for several diameters downstream. At higher frequencies, these eddies which form at the forcing frequency are small and are quickly lost by coalescence. This behaviour is qualitatively consistent with many features of the nonlinear behaviour of forced jets described earlier and we now believe that the similarity between the computation and experiment is not purely coincidental but results from the fact that the real flow has significant axisymmetric large-scale structure of the type we model. From the model we can investigate aspects of that structure which cannot be investigated experimentally and thereby make possible increased understanding of these important flows.

2. A discrete-vortex model of an axisymmetric jet

The jet shear layer is modelled by the superposition of vortex ring elements. We consider first the velocity field of a single vortex ring. We use cylindrical co-ordinates (x, σ, ϕ); where, for an axisymmetric ring, x is the direction of the ring axis, σ is the direction of the ring radius and there is no variation with ϕ, the azimuthal angle about the axis $\sigma = 0$. The Stokes stream function $\psi(x, \sigma)$ of a circular vortex of strength κ at (x', σ') is given by Lamb (1924, art. 161):

$$\psi(x, \sigma) = -\frac{\kappa}{2\pi}(r_1 + r_2)(K(\alpha) - E(\alpha)), \tag{1}$$

where

$$r_1 = ((x-x')^2 + (\sigma-\sigma')^2)^{\frac{1}{2}},$$
$$r_2 = ((x-x')^2 + (\sigma+\sigma')^2)^{\frac{1}{2}},$$
$$\alpha = (r_2 - r_1)/(r_2 + r_1),$$

and $K(\alpha)$ and $E(\alpha)$ are complete elliptic integrals of the first and second kinds.

The components (u, v) of the induced velocity are obtained from the stream function

$$u = -\frac{1}{\sigma}\frac{\partial \psi}{\partial \sigma} \tag{2}$$

and

$$v = \frac{1}{\sigma}\frac{\partial \psi}{\partial x}. \tag{3}$$

Any curved vortex filament has a self-induced velocity. Unless the filament has some finite cross-section, this self-induced velocity is infinite. The self-induced velocity u_c of a ring vortex of small, approximately circular, cross-section is given by Saffman (1970),

$$u_c = \frac{\kappa}{4\pi\sigma'}\left(\ln\frac{8\sigma'}{b} - \tfrac{1}{4} + O\left(\frac{b}{\sigma'}\right)\right), \tag{4}$$

where b is the radius of the cross-section. For constant circulation κ,

$$b = \frac{B}{\sigma'^{\frac{1}{2}}},$$

where B is constant. Therefore equation (4) becomes

$$u_c = \frac{\kappa}{4\pi\sigma'}\left[\ln\left(\frac{8\sigma'^{\frac{3}{2}}}{B}\right) - \tfrac{1}{4} + O\left(\frac{B}{\sigma'^{\frac{3}{2}}}\right)\right]. \tag{5}$$

A value for B must be chosen, and to keep the error term in (5) small we require $B \ll \sigma'^{\frac{3}{2}}$ but apart from this we see that the value of u_c remains relatively insensitive to the choice of B. The size of the core affects not only the value of the self-induced velocity but also the mass of fluid that would be carried along with the vortex ring, cf. Batchelor (1970), figure 7.2.4. These vortex rings are used in our model as elements of the flow in a cylindrical shear layer, with a value of $B = 0{\cdot}001$. That value was chosen so that the body of the fluid moving with an isolated ring element would be small and the self-induced element of the convection velocity was less than one-fifth of the velocity due to all the ring elements in the shear layer. We showed by numerically testing different models that the flow calculation was insensitive to this choice of core parameter. It is a much less critical issue in a problem with an array of vortex rings than it is in the case of a single vortex element though even then the velocity is insensitive to its variation over quite a large range. Nevertheless, the choice is really quite arbitrary, and we can justify it only by the eventual outcome of the calculations. With the computer effort available, we were unable to satisfy exactly the boundary conditions for a jet pipe surface. We instead represented the flow inside it by a long array of identical vortex ring elements. The self-induced convection velocity of such a cylindrical vortex tube was calculated, and these jet-pipe elements were driven at this velocity until they reached the jet-pipe exit plane. At this point, they became part of the jet flow and were free to move under the combined velocity fields of the other jet-flow elements, the jet-pipe elements and of course their own self-induced field. The total number of ring elements in the jet-pipe array was kept constant; new elements were introduced at the upstream end of the jet-pipe array which was sufficiently long for this to have no discernible effect on the jet-flow vortices.

The jet-flow array of elements consisted of a double row of ring elements to provide definition to the large structures which might evolve. The axial spacing of this double row was approximately $0{\cdot}05D$ (where D is the jet-pipe diameter) and the radial

separation was $0{\cdot}025D$. The subsequent position of each ring element was calculated from the total velocity induced on each ring. This velocity was the sum of the self-induced velocity (5), and the total induced by all other vortex elements, computed from equations (2) and (3). The computation time required to calculate these velocities was very large and thus a fairly coarse time-step was used which was held constant throughout the computation. The new position of each vortex ring is given approximately by:

$$\mathbf{x}_i(t+\Delta t) = \mathbf{x}_i(t) + \mathbf{u}_i(t)\,\Delta t + \left(\frac{\partial \mathbf{u}_i(t)}{\partial t}\right)\frac{(\Delta t)^2}{2};$$

therefore

$$\mathbf{x}_i(t+\Delta t) \simeq \mathbf{x}_i(t) + (3\mathbf{u}_i(t) - \mathbf{u}_i(t-\Delta t))\,\tfrac{1}{2}\Delta t, \tag{6}$$

where $\mathbf{x}_i$ is (x_i, σ_i), the position of the ith vortex ring, and $\mathbf{u}_i$ is the corresponding velocity.

The computation time was kept down further by neglecting the velocity field induced by any ring beyond an axial distance of ten ring radii. Calculations showed that the velocity ignored was less than $0{\cdot}15$ % of the self-induced velocity of a ring of equal size, and this would be smaller still beyond ten radii. The effect, though cumulative, is small compared with the total velocity induced by closer ring elements.

As discussed for our two-dimensional model, the digitization of the shear layer causes small-scale instabilities owing to the high velocities induced by neighbouring vortex elements. The smoothing core introduced to suppress this instability is much larger than the core specified to calculate the self-induced velocity of each ring. The smoothing-core radius was defined as a constant fraction (one fifth) of the ring radius, and the velocities within the core were obtained by linearly interpolating along the diameter between the two end points at that radius.

Additional visualization of the jet development was provided by incorporating a streak-line. Inactive elements were introduced at a point outside the shear layer in the jet-pipe exit plane and allowed to move in the induced velocity field of the jet. A check was kept on the maximum and minimum distances between the points on the 'dye' line and elements were added or subtracted in order to maintain reasonable definition. This is equivalent in the experimental situation to allowing the streak-line to stretch or thicken although only the information of the line's position is retained, and of course in our model the 'dye' does not diffuse.

A non-dimensional time parameter T may be defined,

$$T = U_0\, t/D, \tag{7}$$

i.e. the mean jet flows one diameter in one unit of T; U_0 is the centre-line velocity of a cylindrical vortex sheet of strength κ_0 per unit length, i.e.

$$U_0 = \kappa_0.$$

The jet-pipe array was defined with this strength κ_0 per unit length. This jet-pipe array was driven at the convection velocity U_d of such a long vortex tube; and we calculated this velocity to be such that $U_d/U_0 = 0{\cdot}54$. The time-step used in the computation was kept constant at $T = 0{\cdot}0333$.

The effect of forcing was incorporated into the model by causing the driving velocity

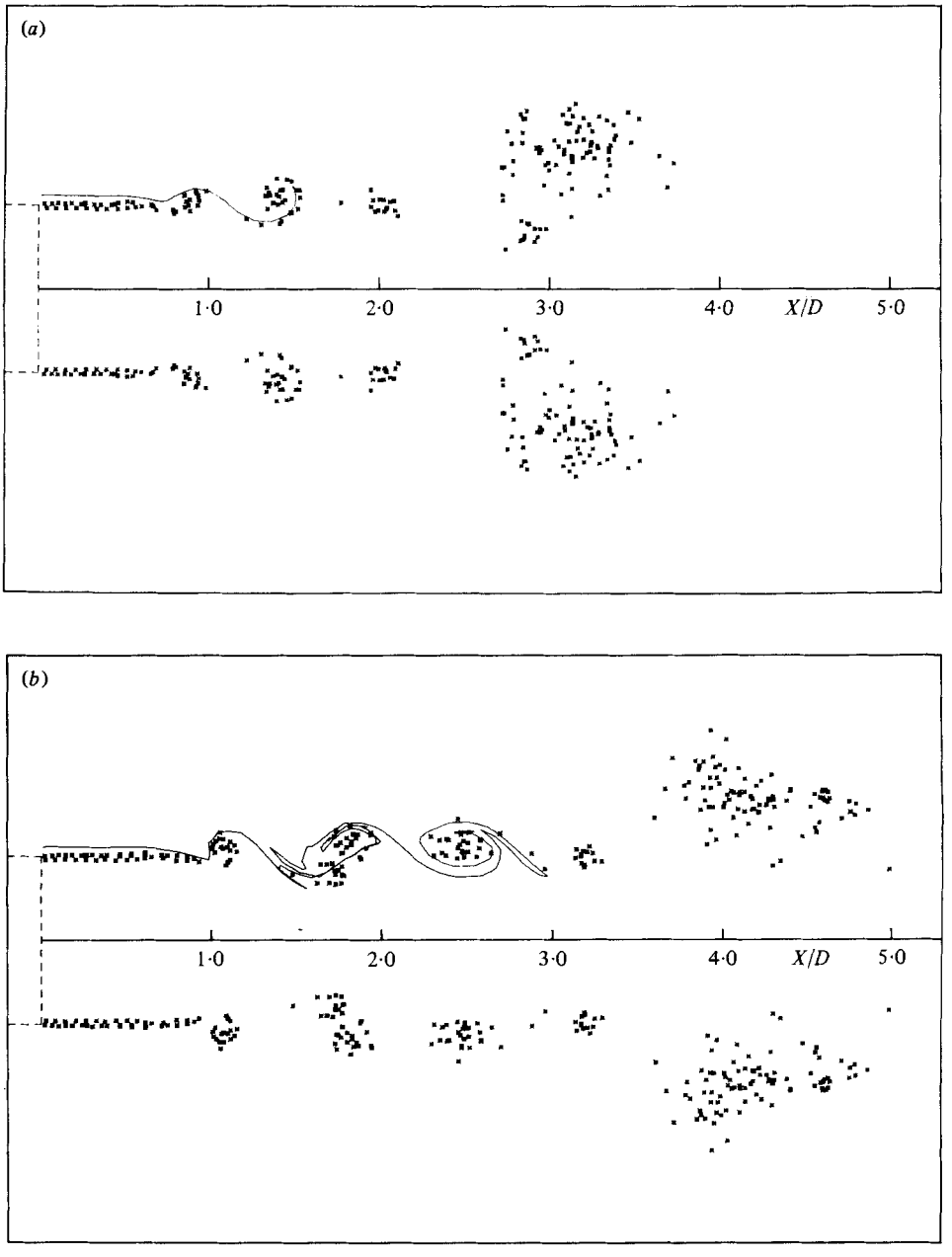

FIGURE 1 (*a*, *b*). For legend see next page.

and strength of the jet-pipe vortices to fluctuate harmonically. The fluctuating strengths and driving velocities were defined

$$\kappa = \kappa_0(1 + A \sin 2\pi ft), \quad U = U_d(1 + A \sin 2\pi ft). \tag{8}$$

At the time each vortex element left the jet pipe, the circulation was fixed at the current value, but of course divided equally between the two elements comprising the

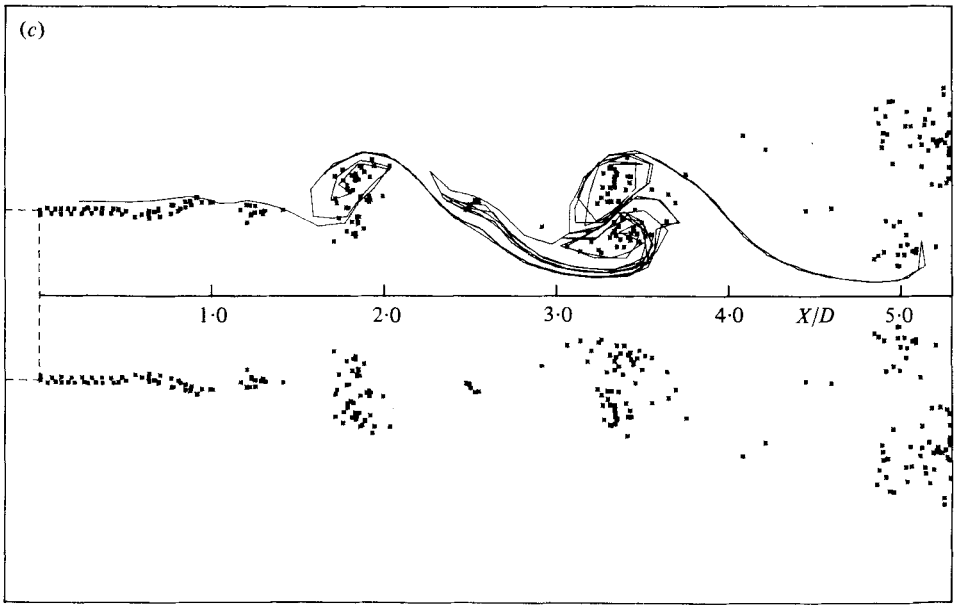

FIGURE 1. The development of an axisymmetric jet represented by discrete vortex elements. (*a*) $T = 8{\cdot}0$; (*b*) $T = 10{\cdot}0$; (*c*) $T = 12{\cdot}0$.——, dye line; *, vortex elements.

double row of the jet flow array. A forcing Strouhal number St was defined as the non-dimensional value of the forcing frequency f,

$$St = fD/U_0. \tag{9}$$

The initial radial separation of the vortex ring elements which leave the jet pipe determines the jet-pipe exit-velocity profile. This profile was not varied and the separation remained constant throughout all the model flows. The resulting velocity profile at the jet-pipe exit is within the range of those measured by Moore (1974) in a study of turbulent jets; he also showed that the jet behaviour beyond $X/D = 1$ (where X is the axial distance from the nozzle exit) was independent of the nozzle profile chosen. That the conditions at the jet-pipe exit are in good agreement with these experimental observations gives confidence that the model jet is not unrepresentative of the real jets. We now consider the subsequent development of this model jet.

3. The results of the unforced model jet

Figure 1(*a*)–(*c*) shows stages in the computed development up to $T = 12{\cdot}0$. The jet-pipe elements are not shown. It can be seen, after the starting vortex has formed, that the instabilities grow on initial shear layer and small clumps, or eddies, form which interact with each other as they move downstream and evolve into larger eddies. At least these qualitative features of a real jet are modelled effectively. The complete evolution of the model jet can be described by a series of such pictures but this is not very useful for quantifying the details of the eddy motion. A possible means of describing that involves the velocities induced by the eddies, and the most useful velocity for this purpose is the radial velocity. Figure 2(*a*) shows the unforced jet

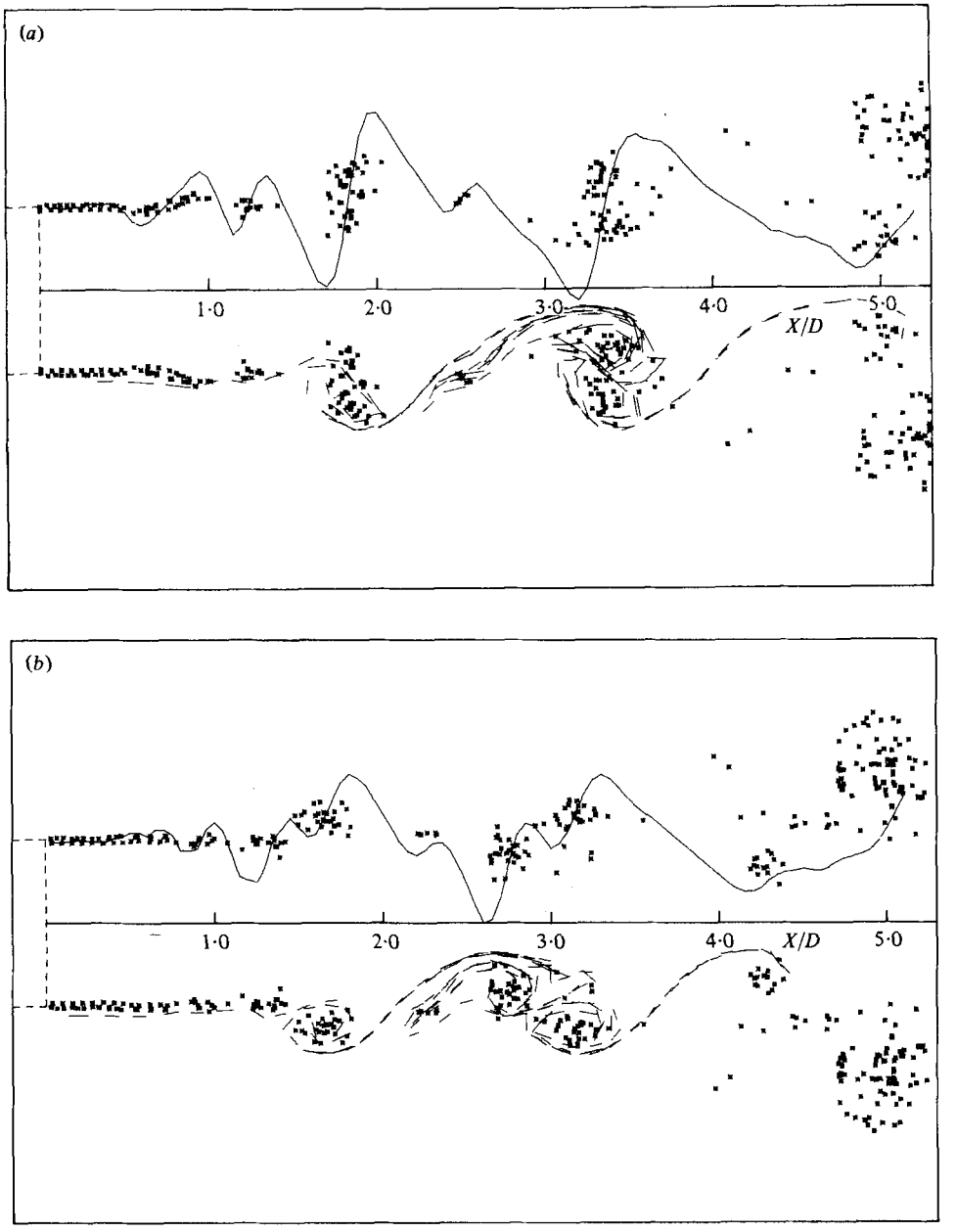

FIGURE 2. A stage in the unforced jet development showing the axial distribution of the induced radial velocity at $R/D = 0{\cdot}5$. (*a*) $T = 12{\cdot}0$; (*b*) $T = 11{\cdot}4$. ——, radial velocity trace; – – –, dye line; *, vortex elements.

development of figure 1 (*c*) with the axial distribution of radial velocity V superimposed. The velocity is measured at $R/D = 0{\cdot}5$, where R is the radial distance from the jet axis, and the velocity is plotted with $V = 0$ along $R/D = 0{\cdot}5$. Every large eddy in the development has a clear effect on the radial velocity; there is a distinct trough before the eddy and a crest after it. The dye-line in the figure indicates that the large eddy

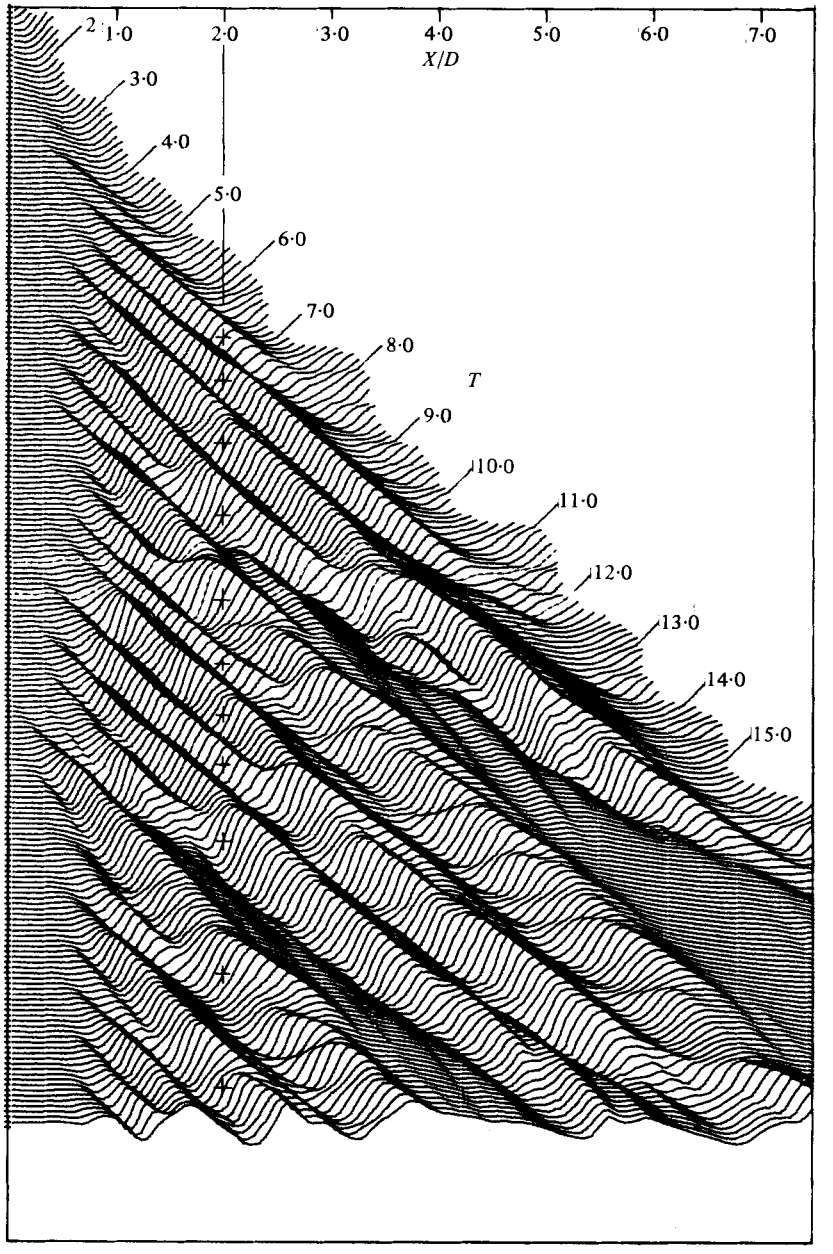

FIGURE 3. The axial distribution of radial velocity at equal time intervals; unforced jet.

located between $X/D = 3$ and $X/D = 4$ has resulted from the coalescence of the two smaller eddies. The development at an earlier time, figure 2(*b*), just before the coalescence, shows the effect on the radial velocity trace. The crest due to the first eddy and the trough of the second are very close together and become indistinguishable once the two eddies have lost their separate identities.

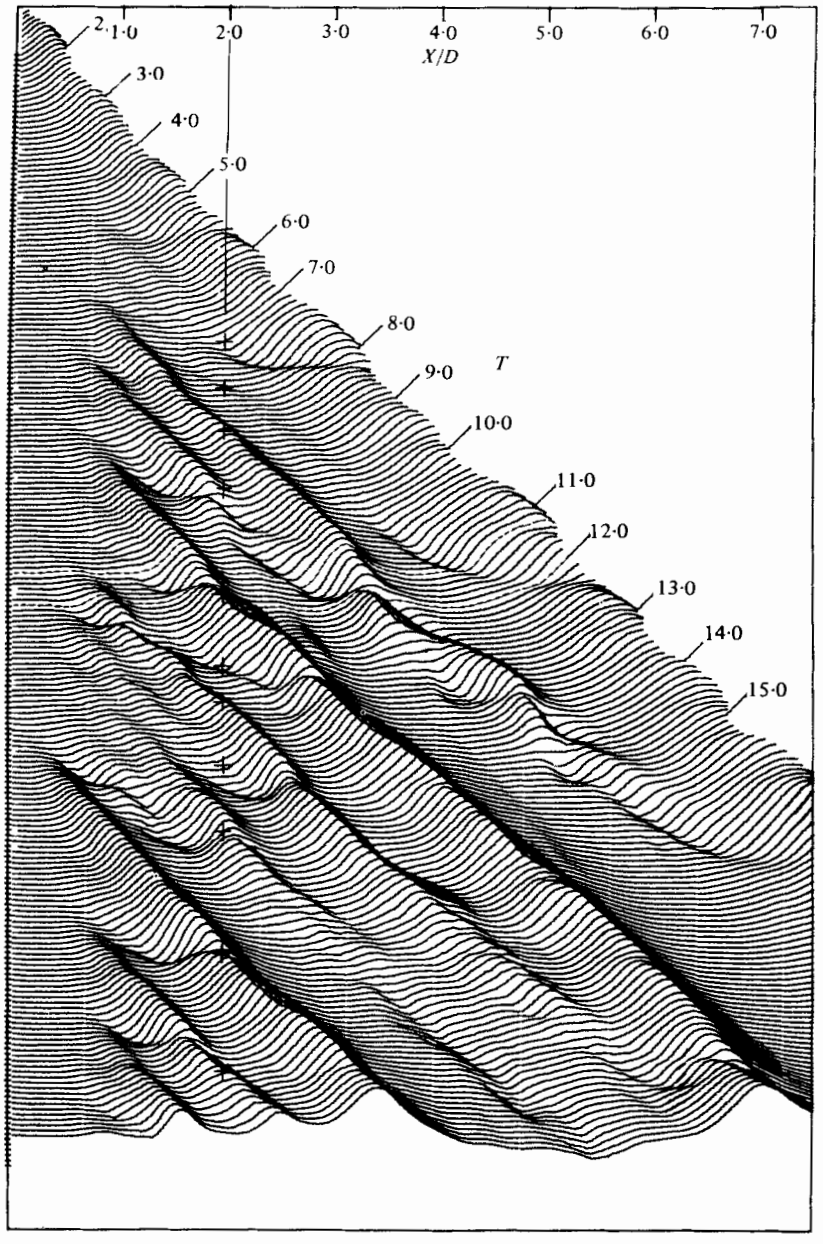

FIGURE 4. The axial distribution of axial velocity at equal time intervals; unforced jet.

These radial velocity traces are calculated at small time intervals during the jet development and then plotted with consecutive origins slightly displaced from each other to form a composite picture of the jet development in which each eddy has a well-defined axial position. This is shown in figure 3, where the radial velocity traces given in figures 2 (*a*) and (*b*) are shown as dotted lines. The traces are plotted at intervals of $T = 0{\cdot}1$ and values of T measured from the start of the jet development are shown.

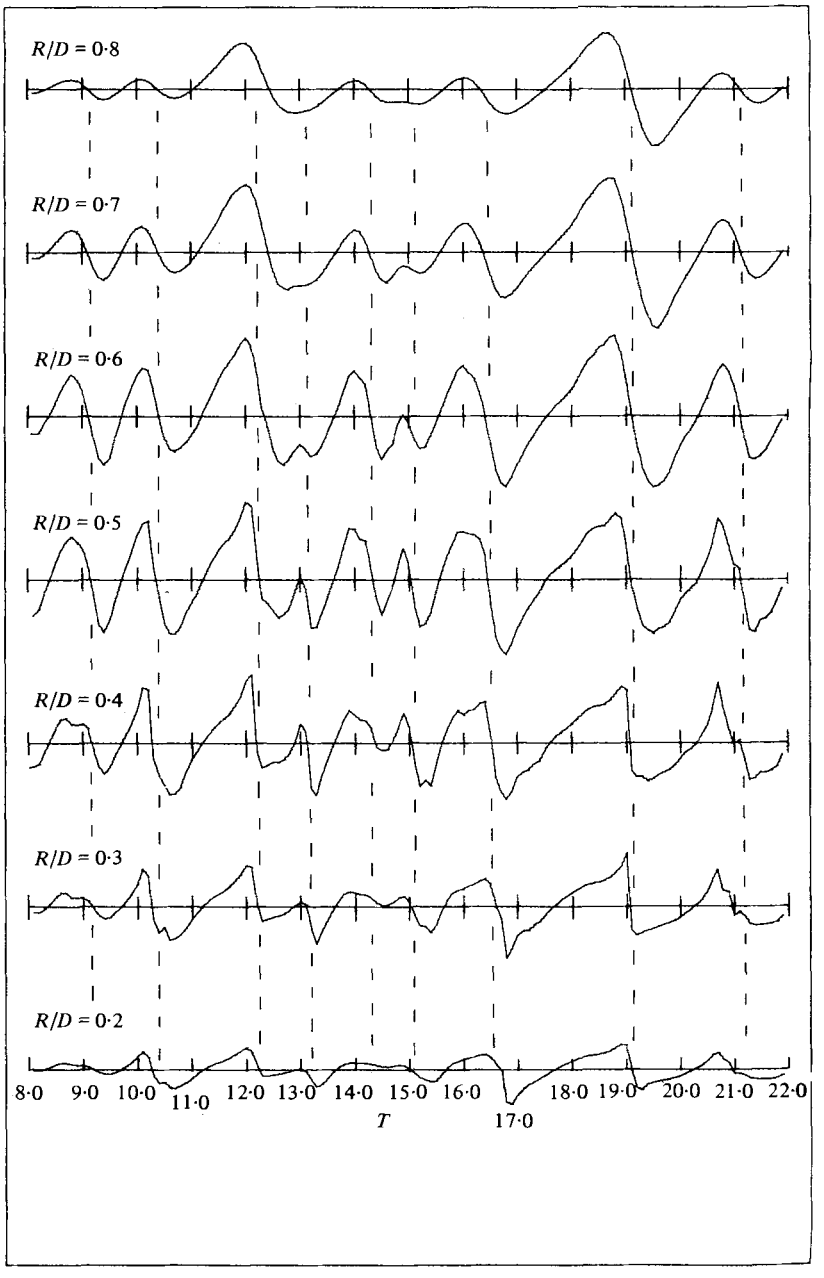

FIGURE 5. Time history of radial velocity fluctuations at $X/D = 2$.
– – –, instants when eddy centres pass.

Each trace is terminated at an arbitrary point in the starting vortex which is thus not shown.

The radial velocity traces in figure 3 show the random pattern of events in the unforced jet development. The plotting scale is such that the crests of the traces, which occur immediately downstream of an eddy, form envelopes of approximately constant

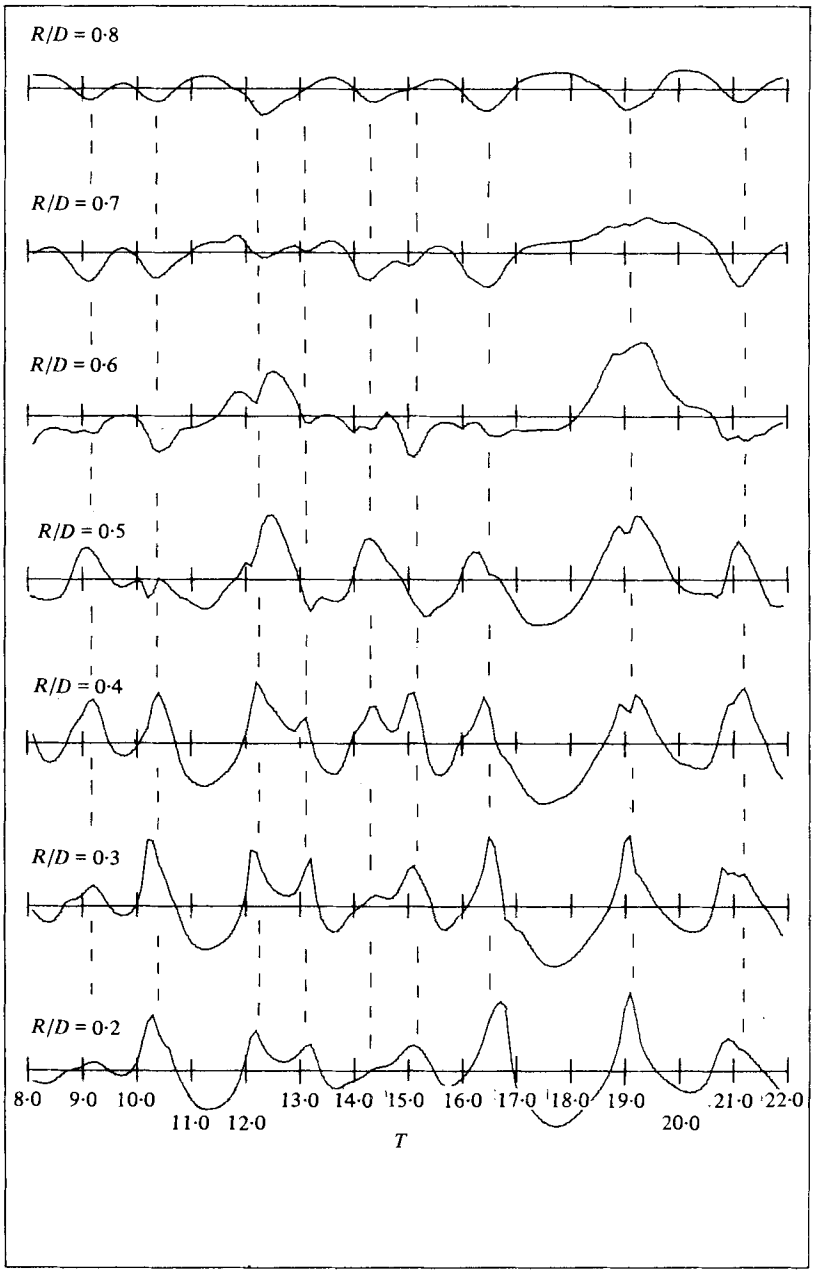

FIGURE 6. Time history of axial velocity fluctuations at $X/D = 2$.
– – –, instants when eddy centres pass.

slope and disappear when two eddies coalesce. This is seen clearly at $T = 11{\cdot}4$ as previously described. The axial spacing between eddies is also apparent and therefore some indication of the relative sizes of the eddies is given. It can also be seen that no distinguishable eddy forms for at least half a diameter downstream of the jet-pipe exit. The line $X/D = 2{\cdot}0$ is shown in the figure and the estimated positions of the eddies at this station are marked with crosses.

The corresponding axial velocity traces calculated at $R/D = 0{\cdot}5$ are shown in figure 4. It is immediately clear that all eddies in the jet development are not represented. A measurement of axial velocities through the centres of vorticity of a series of identical equi-spaced convecting eddies would not distinguish them, and here only when the centres of vorticity are above or below $R/D = 0{\cdot}5$ is there a corresponding crest or trough in the trace. This is shown clearly by the marked eddy positions at $X/D = 2$ (from figure 3). The envelope of the crests represents the positions of the downstream member of a coalescing pair; at this radial position, peaks in axial velocity are only indications of eddy activity.

The fluctuating components v of the radial velocity signals at $X/D = 2$ are shown in figure 5 at $R/D = 0{\cdot}2$–$0{\cdot}8$. It can be seen that owing to the smoothing that is inherent in the jet model, the traces do not have the high frequency 'turbulent' character observed in the hot-wire signals of real jets. The dotted lines indicate the instants when an eddy centre is at this axial position, estimated from figure 3. At $R/D = 0{\cdot}5$, all eddies have a clear effect on the traces whilst, away from the centre of the mixing region, the effect of the smaller eddies becomes less marked. The probability density functions for these signals are approximately symmetrical as found by Moore (1974).

The corresponding fluctuating components u of the axial velocity signals are shown in figure 6. The eddy positions (time) are indicated. In the inner part of the jet ($R/D = 0{\cdot}2$, $0{\cdot}3$) the passage of an eddy of sufficient size causes a sharp increase in axial velocity followed by a less sharp decrease. In the outer part of the region at $R/D = 0{\cdot}8$ the situation is reversed. At $R/D = 0{\cdot}4$, which is further inside the jet than the 'centre' of the eddy, each eddy is distinguished. This is not so at $R/D = 0{\cdot}5$ (as described previously for figure 4); and at $R/D = 0{\cdot}6$ where only the largest eddies would have the major portion of their vorticity outside this position, the peaks are infrequent.

The character of these axial velocity traces can be compared with those found in experimental studies of round turbulent jets. Examples of the time history of hot-wire signals of axial velocity traces at $X/D = 2$ (obtained from X-probe hot-wire system) are given by Lau, Fisher & Fuchs (1972) and described further by Lau & Fisher (1975). At $R/D = 0{\cdot}4$, there were regular downward (negative) spikes occurring at a proposed vortex passing frequency; and at $R/D = 0{\cdot}6$ there were fairly regular upward spikes at approximately one-third of this frequency. The probability density function distribution of the axial velocity at $R/D = 0{\cdot}6$ had positive skew. These features of the axial velocity signals at $R/D \simeq 0{\cdot}6$ are evidently shared by our model. Furthermore, there is qualitative agreement in the symmetry of the probability density function at $R/D = 0{\cdot}5$. However, on the inside of the jet our model does not show the regular downward spikes observed by Lau, Fisher & Fuchs.

The cause of these measured negative spikes is rather unclear. Lau, Fisher & Fuchs suggested that the mixing region consists of a convecting axial array of developing toroidal eddies but that this simple model required some extension because the velocities induced by such a 'basic vortex model' cause no Reynolds shear stress to be generated in the mixing region because each ring induces no axial velocity at this radial position $R/D = 0{\cdot}5$ where the radial velocity is highest. (Actually, this is incorrect; for a ring vortex, the streamlines are not circular and there is an induced positive axial velocity at all axial positions.) The positive spikes at $R/D = 0{\cdot}6$ were

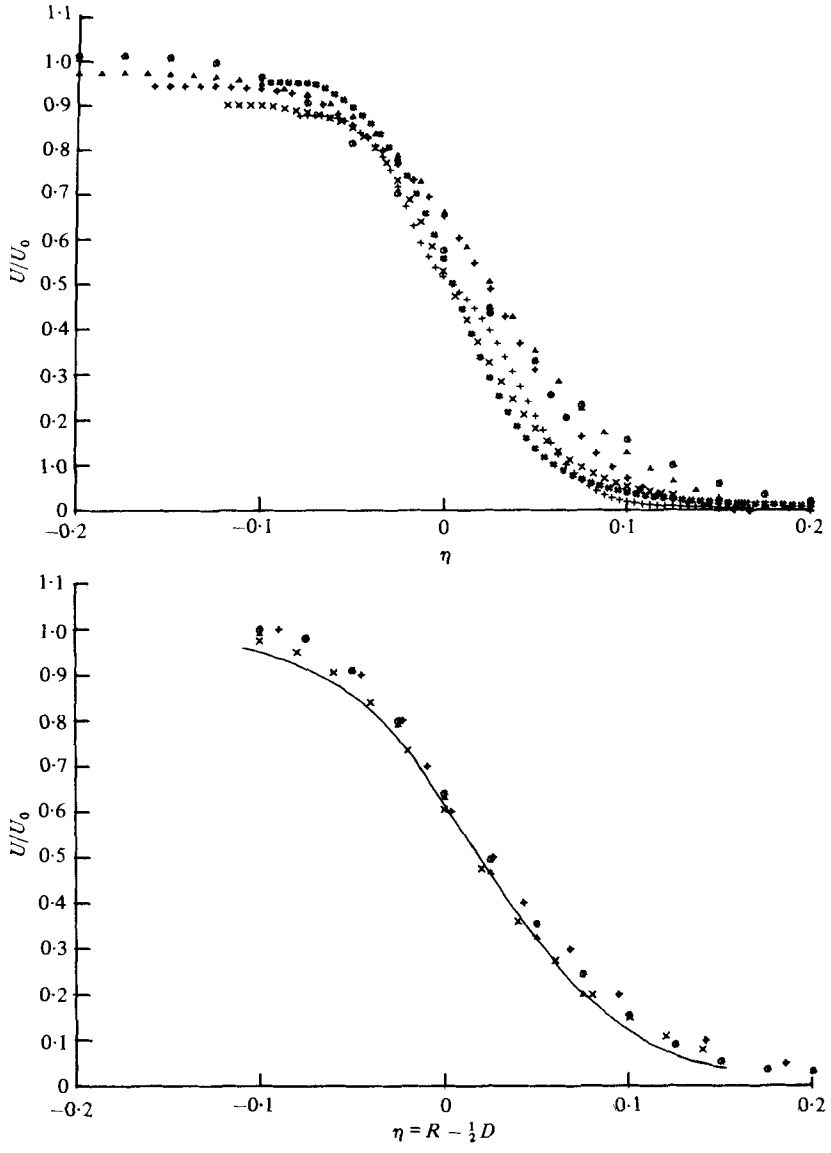

FIGURE 7. The normalized mean velocity profiles of the unforced jet (*a*) and comparison with several experimental studies (*b*). (*a*) ⦶, $X/D = 1{\cdot}0$; △, $X/D = 2{\cdot}0$; ◇, $X/D = 3{\cdot}0$; ×, $X/D = 4{\cdot}0$; #, $X/D = 5{\cdot}0$; +, $X/D = 6{\cdot}0$. (*b*) ⦶, Bradshaw *et al.* (1964), $X/D = 2{\cdot}0$; △, Bradshaw *et al.* (1964), $X/D = 4{\cdot}0$; ◇, Ko & Davies (1971), $X/D = 1{\cdot}0, 4{\cdot}0$; ×, Davies *et al.* (1963), $X/D = 3{\cdot}0$; ——, unforced jet, $X/D = 1{\cdot}0$–$3{\cdot}0$.

explained by the vortex-induced movement of high velocity fluid from the potential core into the low speed side of the mixing region; and the negative spikes at $R/D = 0{\cdot}4$ by the movement of low-velocity fluid from the outer region towards the potential core. However, our model shows that this cannot be the entire explanation, for, if the eddies remain axisymmetric, the necessary proximity to the axis of the vortex sheet as it moves inwards with the outer slower moving fluid causes a rapid downstream

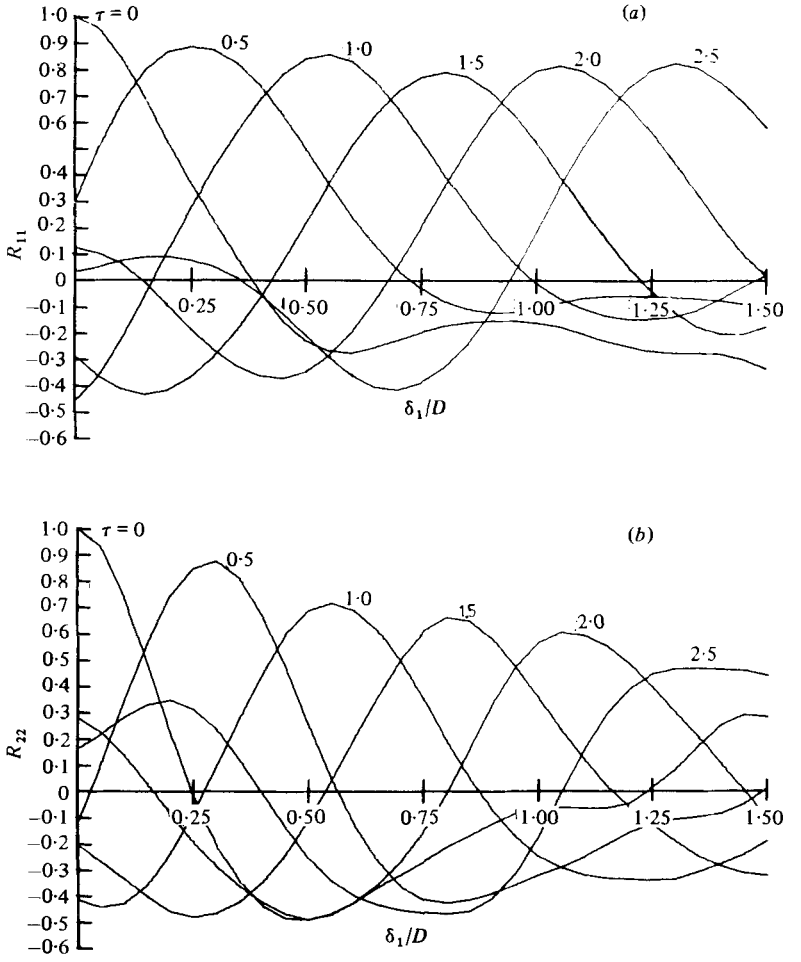

FIGURE 8. The variation of the velocity space–time correlation coefficients with axial separation at $X/D = 2$, $R/D = 0{\cdot}5$. (*a*) $R_{11}(\delta_1, 0, 0)$; (*b*)$R_{22}(\delta_1, 0, 0)$.

acceleration and actually induces positive spikes not negative ones. We conclude that the real case cannot be entirely axisymmetric; we discuss this further in § 5 and show that a rapidly contracting vortex ring is highly unstable and will cease to be axisymmetric.

The mean velocity profiles are calculated by averaging the instantaneous velocities beginning at the time when the starting vortex had moved sufficiently far downstream not to affect the signal. This means that the available data becomes less with increasing downstream distance and therefore, as all data presented here is averaged over a necessarily short time, the data at further downstream stations becomes less reliable. The normalized axial velocity profiles of the unforced model jet are given in figure 7. The profiles cease to be approximately similar beyond $X/D = 3$, a feature consistent with the observation of Bradshaw, Ferriss & Johnson (1964) who found that, for $X/D > 2$, there was an inward displacement of the shear layer. The mean profile for the range $X/D = 1$ to 3 is replotted in the figure and this also seems to be in reasonable agreement with the several experimental studies shown.

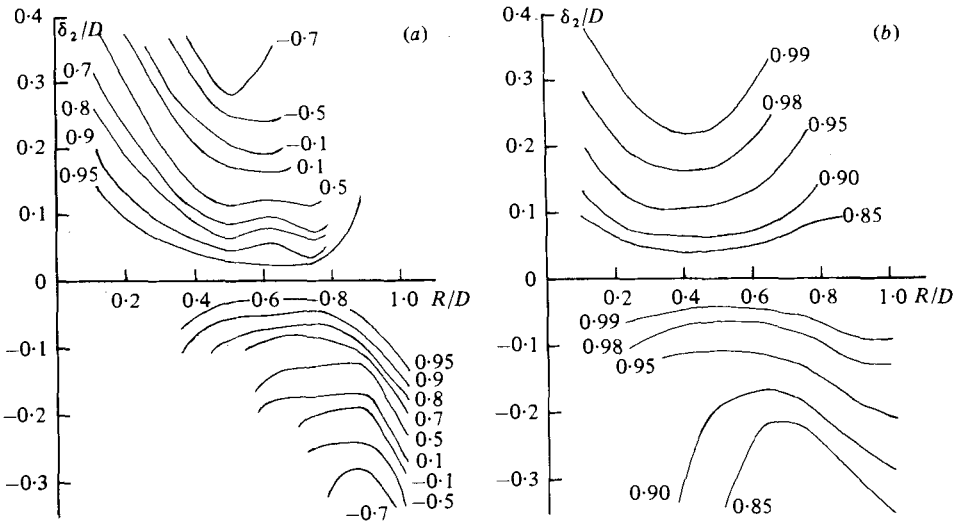

FIGURE 9. Contours of the velocity space correlation coefficients with radial separation at $X/D = 2$. (*a*) $R_{11}(0, \delta_2, 0)$; $R_{22}(0, \delta_2, 0)$.

The r.m.s. values of the fluctuations of the jet velocities were also calculated but in this respect the model is less representative of a real jet because the model is strictly axisymmetric and the radial component must fall to zero on the jet axis. Furthermore the axial component is always greater than the radial component within the potential core. The centre-line 'turbulence' levels are much greater than those measured by Ko & Davies (1971) and Bradshaw, Ferriss & Johnson (1964). Also their measured axial and radial profiles at $X/D = 2$ were found to be approximately equal with the maximum value of $\tilde{u}/U_0 \simeq 0{\cdot}14$ at $R/D \simeq 0{\cdot}5$. For the model jet these magnitudes are larger, the maximum values are $\tilde{u}/U_0 \simeq 0{\cdot}2$ and $\tilde{v}/U_0 \simeq 0{\cdot}25$. The two profiles do not have the same shape: the radial component reaches its peak value further into the mixing region (approximately at the eddy centres, $R/D \simeq 0{\cdot}5$) than the axial component.

Velocity correlation functions are often measured in experimental studies to estimate eddy structures and sizes in the flow. We may estimate these velocity correlation functions for our model jet flow. The velocity space–time correlation coefficient may be defined:

$$R_{ij}(x; \boldsymbol{\delta}, \tau) = \frac{\overline{u_i(\mathbf{x}, t)\, u_j(\mathbf{x}+\boldsymbol{\delta}, t+\tau)}}{\tilde{u}_i(\mathbf{x}, t)\, \tilde{u}_j(\mathbf{x}+\boldsymbol{\delta}, t+\tau)}, \tag{10}$$

where u_i, u_j are fluctuating velocities with zero mean; $\tilde{u}_i$, $\tilde{u}_j$ are the r.m.s. values; τ is the time delay and for the axisymmetric jet $\mathbf{x} = (X, R, 0)$ and the spatial separation $\boldsymbol{\delta} = (\delta_1, \delta_2, 0)$. We consider first these velocity correlations when $\tau = 0$. Values of $R_{11}(\delta_1, 0, 0)$ and $R_{22}(\delta_1, 0, 0)$ at $X/D = 2$, $R/D = 0{\cdot}5$ are plotted against δ_1/D in figure 8 ($\tau = 0$). These may be compared with the values given by Bradshaw, Ferris & Johnson. The magnitudes of the model correlation functions are higher than those observed experimentally, but show similar features: the R_{11} correlation crosses the axis at $\delta/D \simeq 0{\cdot}4$ and remains negative; the R_{22} correlation first crosses the axis at $\delta/D \simeq 0{\cdot}25$ and eventually becomes positive again.

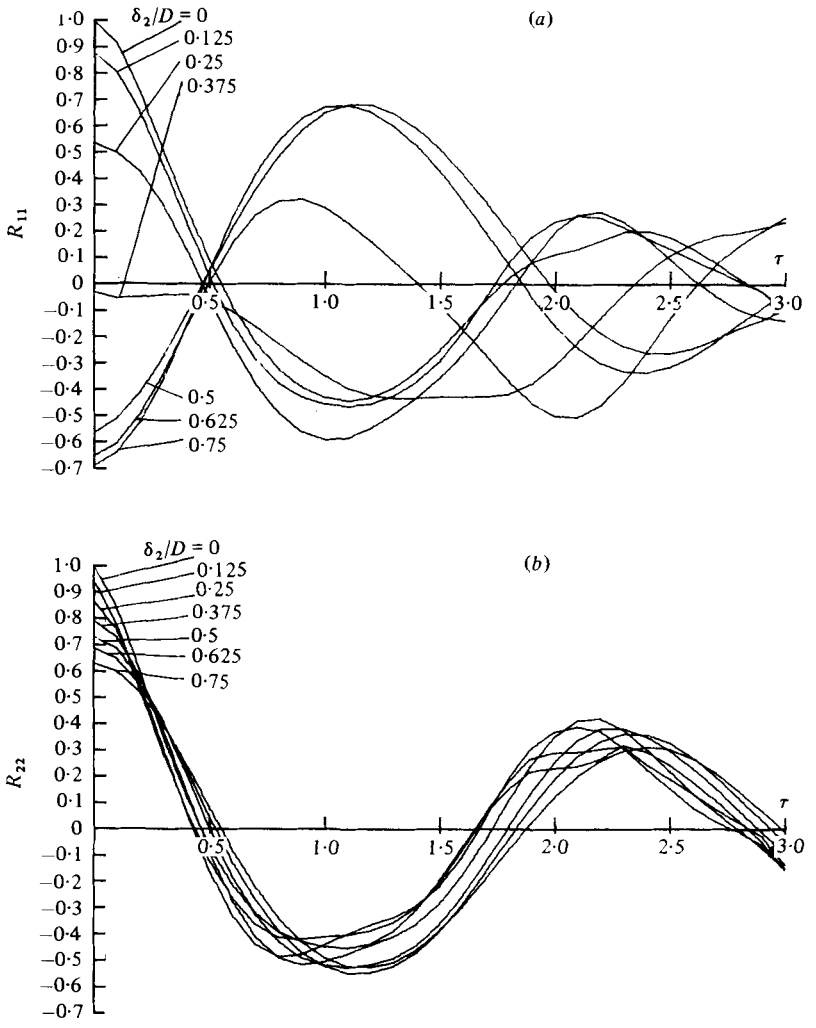

FIGURE 10. The variation of the velocity space–time correlation coefficients (radial separations) with time delay at $X/D = 2$, $R/D = 0{\cdot}25$. (*a*) $R_{11}(0, \delta_2, 0)$; (*b*) $R_{22}(0, \delta_2, 0)$.

Contour plots of $R_{11}(0, \delta_2, 0)$ and $R_{22}(0, \delta_2, 0)$ at $X/D = 2$, for several values of R/D and δ_2/D are shown in figure 9. These plots are an alternative presentation of the information given in figures 5 and 6, and may be compared with the correlations measured by Bradshaw, Ferriss & Johnson. Again, the magnitudes of the correlation functions are much larger for the model jet. The model radial velocity signals remain more correlated across the mixing region than those observed by Bradshaw, Ferriss & Johnson; in neither case do they take negative values. Both the modelled and experimentally observed axial velocity signals are well correlated within the mixing region, but the two are quite different across the mixing region. The changes with time of these axial and radial velocity fluctuations across the mixing region are shown in figure 10 where the space–time correlation coefficients $R_{11}(0, \delta_2, 0; \tau)$ and $R_{22}(0, \delta_2, 0; \tau)$ at $X/D = 2$, $R/D = 0{\cdot}25$, are plotted against τ. The correlations are qualitatively very similar to those measured by Lau, Fisher & Fuchs, who suggested that these results

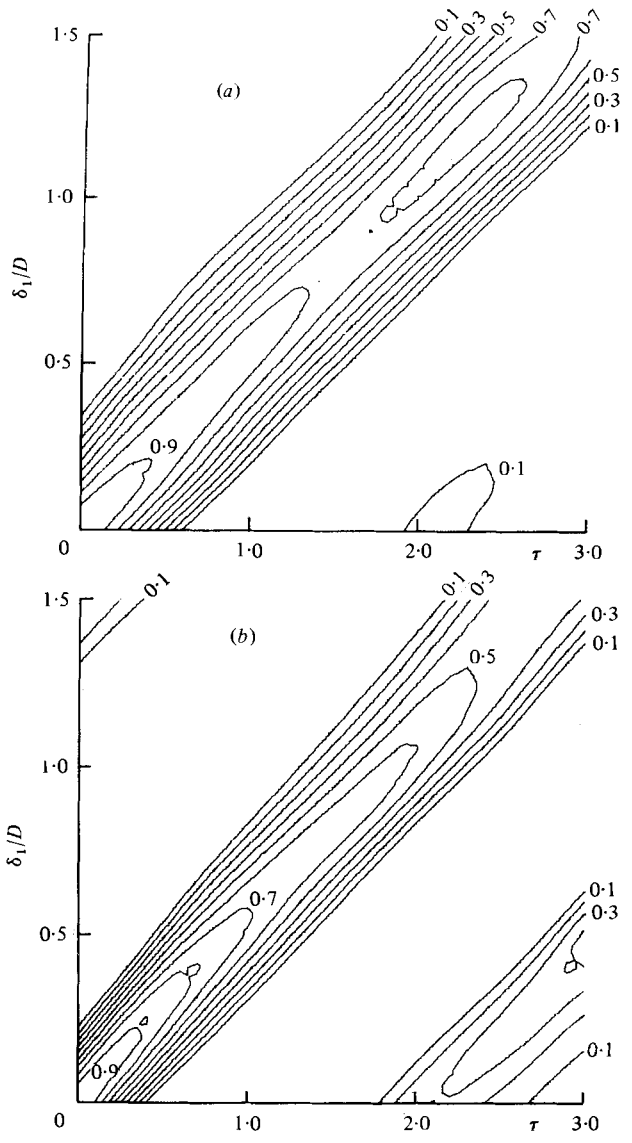

FIGURE 11. Contours of the velocity space–time correlation coefficients at $X/D = 2$, $R/D = 0{\cdot}5$. (*a*) $R_{11}(\delta_1, 0, 0)$; (*b*) $R_{22}(\delta_1, 0, 0)$.

confirmed their proposed extended vortex model. However, the disagreement between our model jet correlations and those measured by Bradshaw, Ferriss & Johnson does confirm some discrepancy in the axial velocity signals in the jet core; this will be discussed further in § 5.

The space–time correlation coefficients with axial separation, $R_{11}(\delta_1, 0, 0; \tau)$ and $R_{22}(\delta_1, 0, 0; \tau)$ which are shown plotted against δ_1/D in figure 8 show many of the features described by Townsend (1976); e.g. the height of the maxima of the curves becomes less with increasing time delay τ, although this effect is more marked for the R_{22} correlation. The radii of curvature with respect to the maxima become greater with

increasing time delay and the variation about the maxima becomes more asymmetric. The R_{22} correlation has a narrower variation about the maxima than the R_{11} correlation which is in agreement with the measurements of Wills (1964). However, the correlations measured by Wills (also at $X/D = 2$, and $R/D = 0{\cdot}5$) are much weaker and both correlations fall much more rapidly with τ than those shown here. We have found that the correlation coefficients for the model jet are higher than those measured experimentally. This is probably due to the much 'cleaner' signals found here, as explained earlier, because the small scales are smoothed in our model. From the previous discussion with regard to the velocity traces in figures 3 and 4, it can be seen that the R_{22} correlation is a more realistic representation of the eddy behaviour. These eddies are changing with time although not rapidly owing to the small-scale smoothing. The axial velocities, however, are only picking out particular eddies which in fact provide a less changeable pattern of turbulence and therefore the correlations remain higher.

Figure 11 shows contour plots of these correlations in which the more rapid fall and the periodic nature of the R_{22} correlations is clear. The regular convecting pattern of axial and radial velocity signals is shown by the diagonal 'bands' in the contour plots. In the R_{22} plot there is a second weakly correlated band which indicates the temporal periodicity in the unforced jet at this axial position. The time delay between the maximum values of R_{22} in these bands $\Delta\tau \simeq 2{\cdot}1$, which is a 'natural' frequency of $St \simeq 0{\cdot}47$.

We may use these space–time correlations to estimate the eddy-connection velocity U_c. The definition most usually adopted is

$$U_c = \delta_1/\tau_1 \quad \text{at} \quad \left(\frac{\partial R(\delta_1, 0, 0; \tau)}{\partial \delta}\right)_{\tau_1} = 0, \tag{11}$$

which is assumed to be approximately independent of τ.

Averaging the calculated velocities over 26 values of τ_1, we found from the axial velocity correlations that $U_c/U_0 \simeq 0{\cdot}52$ and from the radial velocity correlations $U_c/U_0 \simeq 0{\cdot}55$. There is less variation with τ_1 in those velocities calculated from the radial velocity correlations; this was also observed in experiments by Wills (1964). The convection velocities for the modelled jet can also be obtained directly from an x–t plot for the eddy positions. The average convection velocity calculated from such a plot is $U_c/U_0 \simeq 0{\cdot}56$. Wills measured convection velocities from the space–time correlation coefficients and found that at $X/D = 2$, $R/D = 0{\cdot}5$, from the radial velocity correlations $U_c/U_e = 0{\cdot}65$ which was equal to the local mean velocity, and from the axial velocity correlation $U_c/U_e = 0{\cdot}61$. (U_e is the jet exit velocity.) Ko & Davies (1971) estimated the convection velocity from the axial velocity correlations, using a different definition to equation (11), and found $U_c/U_e = 0{\cdot}58$ at $X/D = 1{\cdot}5$, $R/D = 0{\cdot}5$. At other radial positions in the mixing region, Wills showed that the convection velocity measured from the radial velocity correlations remained approximately constant across the mixing region, whereas that calculated from the axial velocity correlation was much closer to the local mean velocity. As discussed previously, the radial velocities distinguish each eddy and do not change phase across the mixing region and thus should give a constant convection velocity. We see that the estimated convection velocities for our model jet are much lower than those measured in real jets, and also lower than the local mean velocity $\overline{U}/U_0 = 0{\cdot}65$.

In this section we have compared the velocity profiles and correlations of our model

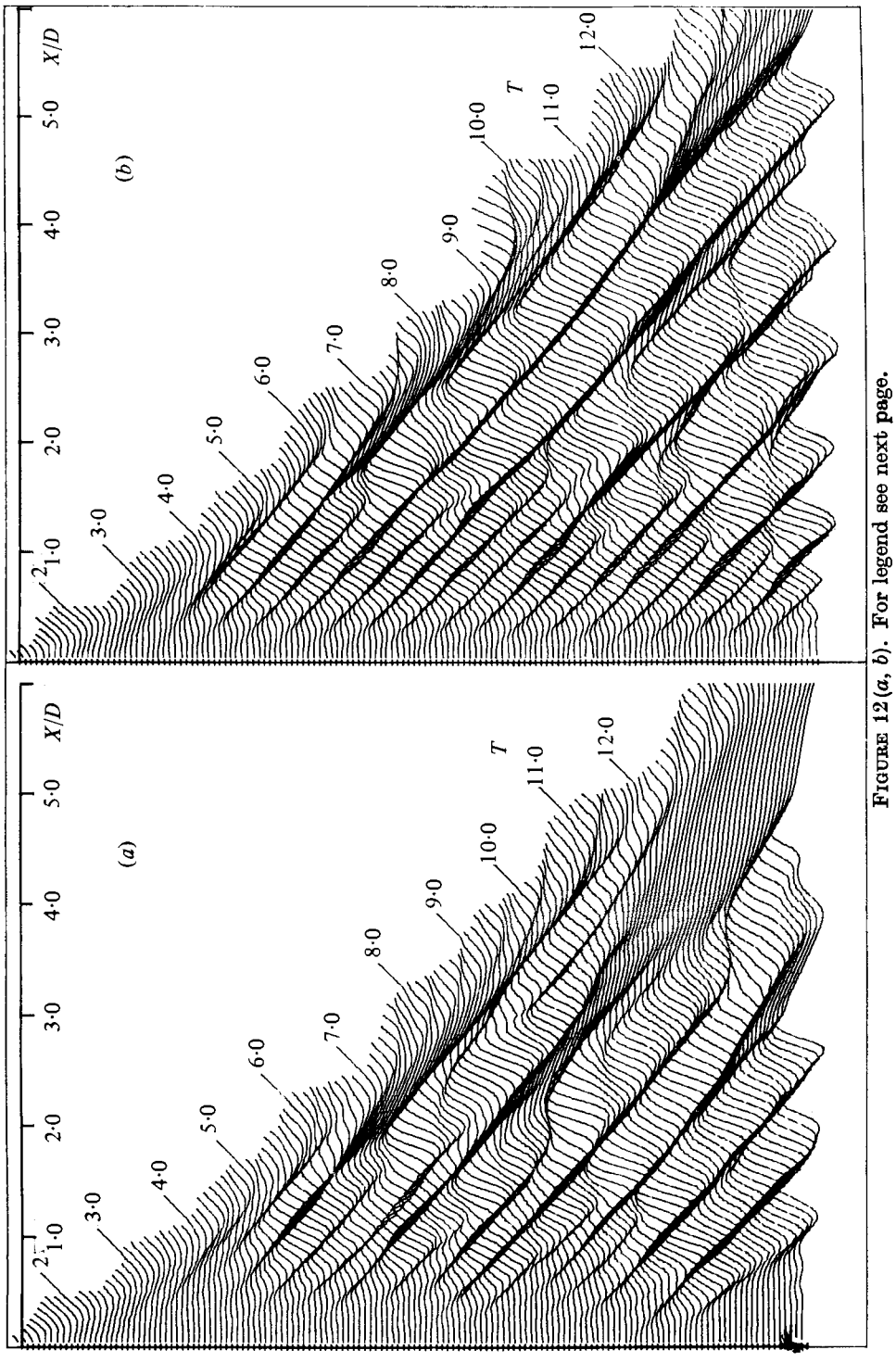

FIGURE 12 (*a*, *b*). For legend see next page.

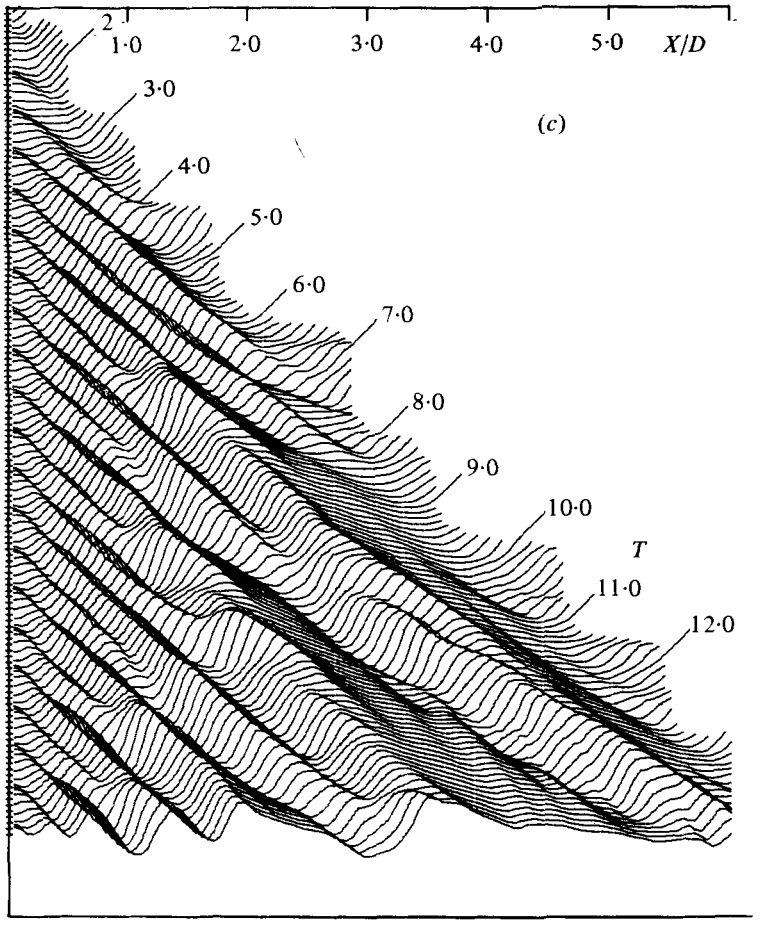

FIGURE 12. The axial distribution of radial velocity at equal time intervals. St = 1·5. (*a*) A = 0·005; (*b*) A = 0·02; (*c*) A = 0·01.

jet with the results of many previous experimental studies. We have shown that there is in general good qualitative agreement but there are differences in the velocity signals in the jet core which may be because the model jet is strictly axisymmetric. However, the model jet does reproduce many features of real jets and so we feel that we can attempt to use the model to investigate in detail the effect of harmonic forcing on the jet development.

4. The results of the forced model axisymmetric jet

The forcing parameters, the amplitude A and Strouhal number St are defined in equations (8) and (9). The effect of three different values of the amplitude A = 0·005, 0·02, 0·1 is investigated at Strouhal numbers of St = 0·1, 0·3, 0·5, 1·5, 2·0. The effect of the forcing on the formation of eddies in the jet may first be quantified by considering the development of the radial velocity traces with time. This is shown in figure 3 for the unforced jet where the eddy formation is irregular with larger eddies forming by coalescence. The effect of forcing on the jet is in general to regularize this development: there is some response to the forcing frequency and this response is usually more marked with increasing amplitude.

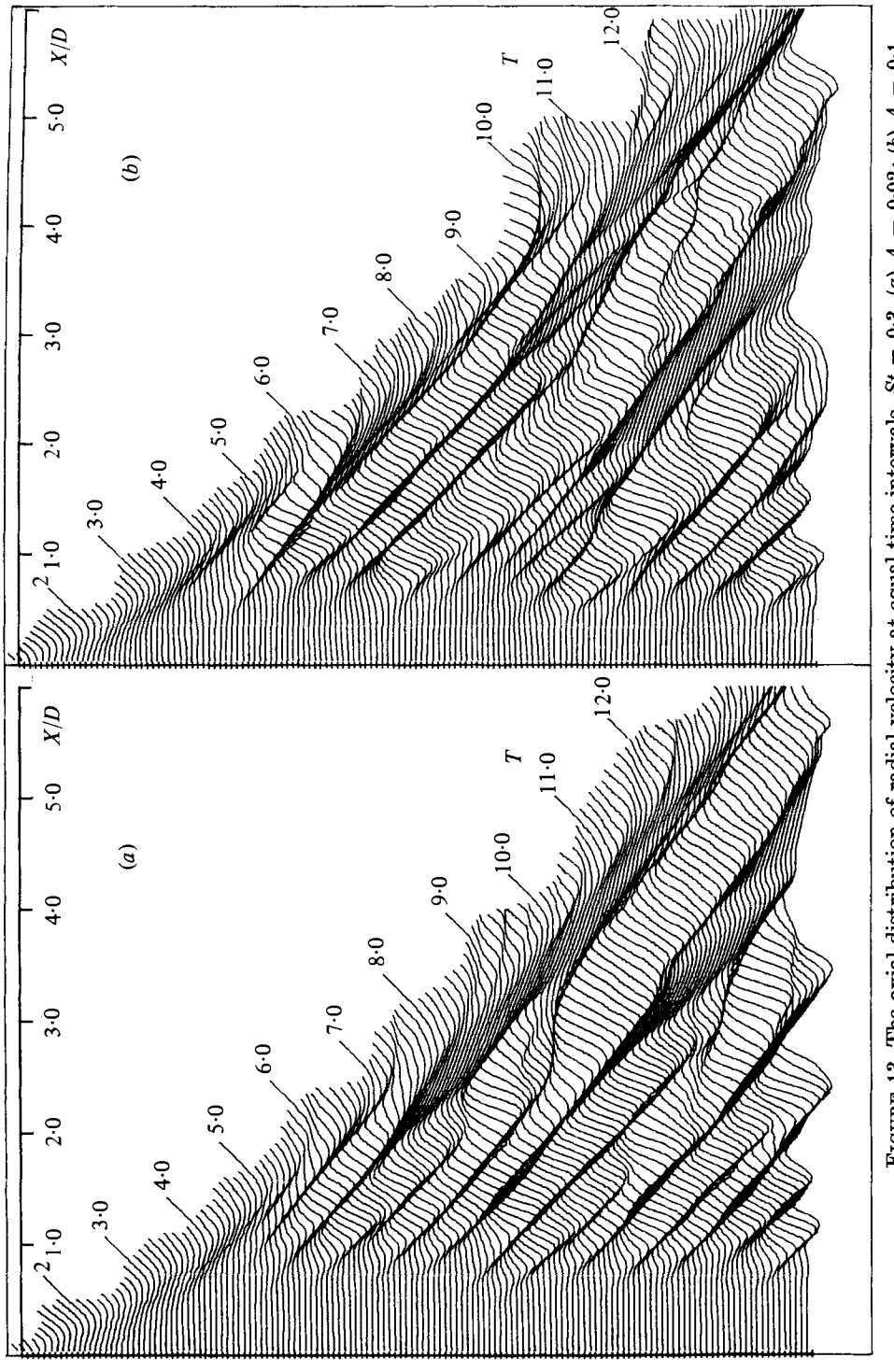

FIGURE 13. The axial distribution of radial velocity at equal time intervals. $St = 0{\cdot}3$. (*a*) $A = 0{\cdot}02$; (*b*) $A = 0{\cdot}1$.

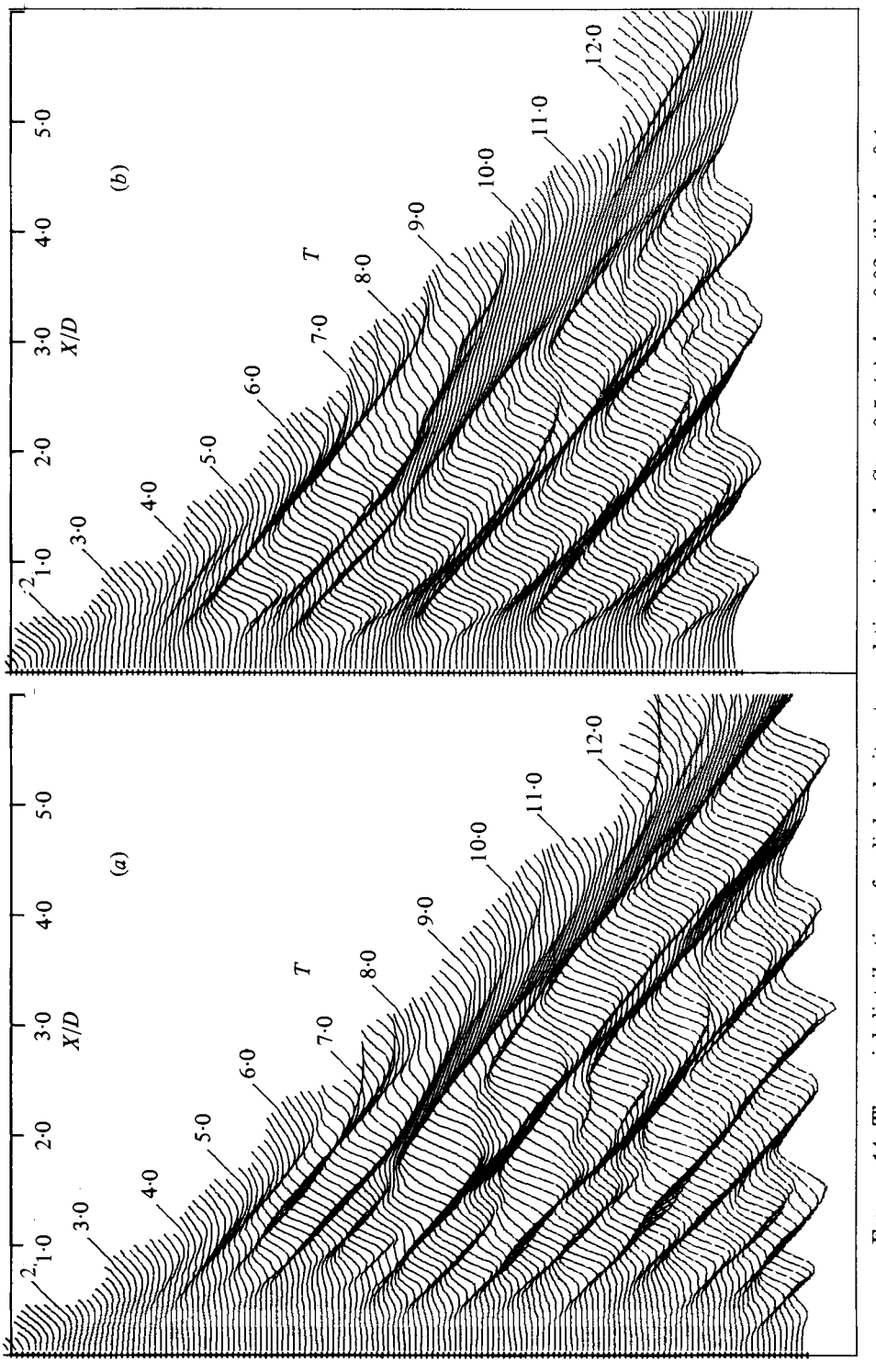

FIGURE 14. The axial distribution of radial velocity at equal time intervals. $St = 0{\cdot}5$. (*a*) $A = 0{\cdot}02$; (*b*) $A = 0{\cdot}1$.

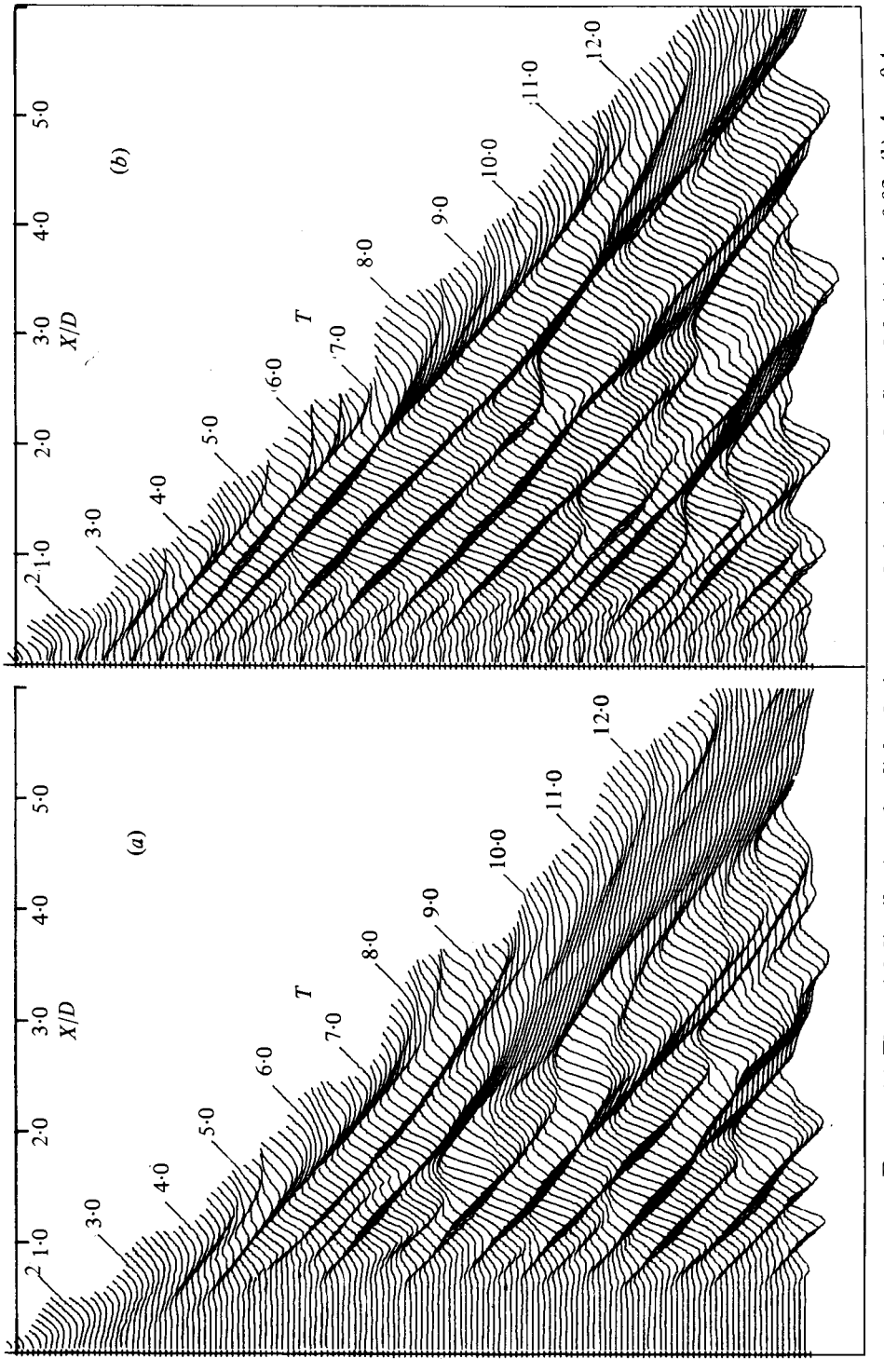

FIGURE 15. The axial distribution of radial velocity at equal time intervals. $St = 2{\cdot}0$. (*a*) $A = 0{\cdot}02$; (*b*) $A = 0{\cdot}1$.

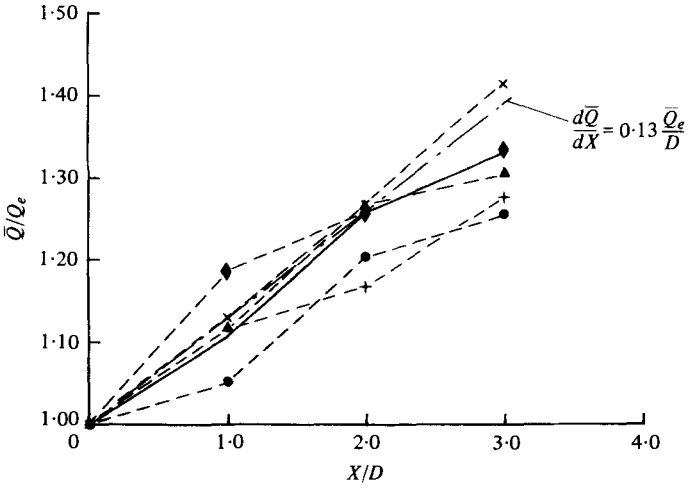

FIGURE 16. The effect of Strouhal number variation on the normalized mean volumetric flow rate. Forced jet, $A = 0{\cdot}1$: ●, $St = 0{\cdot}1$; ▲, $St = 0{\cdot}3$; ◆, $St = 0{\cdot}5$; ×, $St = 1{\cdot}5$; +, $St = 2{\cdot}0$.

Figure 12 shows the time history of the model jet forced at a frequency $St = 1{\cdot}5$ and amplitudes $A = 0{\cdot}005$, $0{\cdot}02$ and $0{\cdot}1$. This frequency corresponds to a forcing wavelength $\lambda/D \simeq 0{\cdot}37$, assuming a convention velocity $U_c/U_0 \simeq 0{\cdot}56$. At the lowest amplitude, shown in figure 12(*a*), it can be seen that the response is slight: the smallest eddies form slightly nearer the nozzle than in the unforced jet, but the development remains irregular. However, with increased amplitudes shown in figures 12(*b*) and (*c*), the jet development becomes more ordered and the initial eddies form regularly near the nozzle at approximately the forcing frequency. This is a small eddy size which cannot be maintained and larger eddies form from regular coalescence at $X/D \simeq 1$ and further irregular pairings occur beyond that. Comparison with figure 3 shows that this initial eddy size is within the range of those present in the unforced jet and therefore a sensitivity to forcing at this frequency is likely.

However, at very low frequencies the jet cannot respond at the forcing frequency. When $St = 0{\cdot}1$, the forcing wavelength would be greater than five diameters which would not be a feasible eddy spacing. The development for $St = 0{\cdot}3$ (forcing wavelength $\lambda/D \simeq 1{\cdot}8$) at a forcing amplitude $A = 0{\cdot}02$ is shown in figure 13(*a*). The response is similar to that when $St = 0{\cdot}1$ (not shown). The jet appears initially more stable and the development is more ordered than in the unforced jet. When the forcing amplitude is higher, $A = 0{\cdot}1$, shown in figure 13(*b*), the development appears very irregular, but a large eddy spacing is finally reached which is near the forcing wavelength.

As the forcing wavelength is shortened the jet shear layer is more sensitive. Figure 14 shows the jet development at a forcing frequency $St = 0{\cdot}5$. At the lower amplitude shown $A = 0{\cdot}02$, the initial eddies form at $X/D \simeq 0{\cdot}6$ with larger spacings than in the unforced jet. There are single pairings and the final spacing corresponds approximately to the forcing wavelength ($\lambda/D \simeq 1{\cdot}1$). When $A = 0{\cdot}1$, figure 14(*b*), the eddy formation is very regular and there is an immediate big-eddy structure at approximately the forcing wavelength.

At higher frequencies, as we have already seen for $St = 1{\cdot}5$ (figure 12), the initial

eddies form at the forcing frequency but soon coalesce to form longer wavelengths. The development for a forcing frequency $St = 2{\cdot}0$ is shown in figure 15. When $A = 0{\cdot}02$, the small eddies form at $X/D \simeq 0{\cdot}8$ with a shorter spacing than in the unforced jet and a resulting smaller large eddy spacing. At $A = 0{\cdot}1$ there is a much stronger response at the forcing wavelength ($\lambda/D \simeq 0{\cdot}28$) which is very small and these eddies have disappeared within one diameter. There are several subsequent pairings to give a large eddy spacing which is slightly shorter than in the unforced jet.

The effect of forcing on the development of the mean velocity profiles and 'turbulence' levels was mostly dependent on the local eddy size at any particular axial position, and not a consistent trend for each Strouhal number. The volume flux $\bar{Q}$ is calculated from the axial velocity profiles: the profiles to be integrated were estimated from using the method suggested by Crow & Champagne. The resulting volume fluxes are normalized with respect to the mean exit value and the axial development is shown in figure 16. The features of the eddy development already described are again apparent. When $St = 0{\cdot}1$, the jet is much less developed than the unforced jet, and the rate of entrainment $d\bar{Q}/dX$ is lower. The entrainment rates of the forced jets relative to the unforced jet vary with axial position. When $St = 0{\cdot}5$, the rate is initially higher but then falls at $X/D = 2{\cdot}0$. Crow & Champagne measured these rates of entrainment for $St = 0{\cdot}3$ and the unforced jet. They showed that, at $St = 0{\cdot}3$, there is a consistently larger entrainment rate than the unforced jet. There is, however, no such behaviour observed here. Crow & Champagne confirm the value that $d\bar{Q}/dX = 0{\cdot}13\bar{Q}_e/D$ for $X/D \lesssim 2$. This constant value is shown on figure 16 and it can be seen that there is good agreement with the entrainment rate of the unforced jet.

The eddy convection velocities for these forced jets were calculated from x–t plots and also from the R_{11} and R_{22} correlations at $X/D = 1{\cdot}0$ and $X/D = 2{\cdot}0$. These were calculated the same way as the unforced jet using equation (11). Overall, the average convection velocity was $U_c/U_0 \simeq 0{\cdot}54$, which was not frequency dependent.

5. Discussion

The development of a round jet was modelled by an inviscid axisymmetric model flow. A major complication of this model was the representation of the nozzle flow. It was not possible to satisfy exactly the nozzle boundary conditions and instead the jet pipe flow was represented by the field of discrete vortex ring elements; this is an enormous idealization of the real case. In principle, this problem can be done exactly. Green's function for the pipe is needed; this was given by Levine & Schwinger (1948). However, it exists in integral form only and the computation time required to use it would be prohibitive. In his experiments on turbulent jets, Moore (1974) showed that the large eddy structure and the jet development beyond $X/D = 1$ were independent of nozzle geometry. Because the jet-pipe exit-velocity profile of our model was within the range of nozzle exit profiles studied by Moore, we feel that our choice of approximation for the nozzle flow was sufficient.

Our model flow was axisymmetric. This seemed not unrealistic since Moore (1977) had shown that an unforced jet had important axisymmetric and first-order modes; and when excited appeared entirely axisymmetric. Also Batchelor & Gill (1962) showed that a thin cylindrical shear layer amplifies axisymmetric waves but a thicker shear layer is more unstable to sinuous waves; this indicated that an axisymmetric model would be appropriate to the early mixing region of a circular jet.

A smoothing core had to be applied to each vortex ring element in the jet flow to suppress the small-scale instabilities caused by the high velocities induced on closely neighbouring vortex elements. This limited the model to the large-scale motions but it is these large eddies which have been shown to be important in many experiments. The large eddy motion is known to be essentially inviscid (Townsend 1976) but the absence of viscosity and the axisymmetry of the model does mean that certain important elements in turbulence were not represented. There was no diffusion of vorticity and hence entrained irrotational fluid remained irrotational and areas of potential flow existed in the model where they are known to be impossible. The model contained no streamwise component of vorticity, which is important in the cascade of energy transfer to the smallest scales. However, although certain aspects of real turbulence are absent in our model, we think that we have modelled correctly many aspects of the large-eddy motion which determine the mean flow in the jet.

Actually, in many respects the qualitative agreement of the results with many experimentally observed flows is good. The normalized mean velocity profiles of the unforced jet given in figure 7 are in reasonable agreement with several experimental studies shown. There is agreement between the initial entrainment rate for the unforced jet and the measurements of Crow & Champagne (1971). This indicates that the entrainment process in the initial stages of the jet development, at least, is essentially inviscid, and small-scale mixing is unimportant. This was observed by Dimotakis & Brown (1975) in a water mixing layer visualized by dye, when the entrained fluid penetrated far into the mixing layer before any small-scale mixing occurred and remained associated with the large-scale motion. As we have shown in our two-dimensional model of eddy coalescence (Acton 1976), the ideas of Brown & Roshko (1974) that entrainment involved the trapping of irrotational fluid between pairing eddies seem entirely plausible. The initial violent roll up of the initial shear layer when the forcing amplitude was high at $St = 0{\cdot}5$ was sufficient to produce a high entrainment rate without pairing as shown in figure 16. However, as the eddy did not increase in size further, this rate decreased downstream of the eddy formation.

The velocity space–time correlations in the mixing layer showed many of the features described by Townsend (1976). There was good agreement in the velocity space–time correlation coefficients across the mixing region with the measurements of Lau *et al.* (1972); this is despite the discrepancy between their measurements and our model axial velocity signals on the inside of the jet. The velocity space correlation coefficients showed many of the features observed by Bradshaw *et al.* (1964) but the axial velocity signals correlated across the mixing region were quite different. There is evidence that the flow on the jet core is not correctly modelled, for example the axial velocity signals observed by Lau, Fisher & Fuchs showed regular negative spikes which are not apparent in our unforced model results (figure 6). The complete reason for this discrepancy remains unclear, but it is possible that this difference might be caused by the real jet losing its axisymmetry near the jet axis. As a large eddy transports fluid towards the potential core of the jet, the entrained vortex ring elements contract. It is possible that this contraction is unstable and leads to a lack of axisymmetry, in the real jet core, which has not been modelled.

We can investigate this for an isolated vortex element and compare the relative stability of contracting or expanding flows. We consider the changes in the radial component of vorticity caused by small radial perturbations in the ring geometry when

the ring moves under the influence of a source (or a sink) at its centre. This is a model of an expanding (or contracting) axisymmetric element of shear layer vorticity. The vorticity equation for inviscid flow is given by Batchelor (1970, ch. 5):

$$\frac{D\boldsymbol{\Omega}}{Dt} = (\boldsymbol{\Omega}.\nabla)\,\mathbf{u}. \tag{12}$$

The vorticity $\boldsymbol{\Omega}$ may be written as the sum of a mean fluctuating component

$$\boldsymbol{\Omega} = \bar{\boldsymbol{\Omega}} + \boldsymbol{\Omega}',$$

and similarly the velocity $\mathbf{u}$ may be written

$$\mathbf{u} = \bar{\mathbf{u}} + \mathbf{u}'.$$

We obtain the equation for the perturbation from (12)

$$\frac{D\boldsymbol{\Omega}'}{Dt} = (\bar{\boldsymbol{\Omega}}.\nabla)\,\mathbf{u}' + (\boldsymbol{\Omega}'.\nabla)\,\bar{\mathbf{u}}, \tag{13}$$

neglecting higher-order terms. We express (13) in cylindrical polar co-ordinates (x, σ, Φ) with unit vectors $(\mathbf{e}_x, \mathbf{e}_\sigma, \mathbf{e}_\Phi)$, noting that

$$\bar{\mathbf{u}} = \frac{m}{\sigma}\mathbf{e}_\sigma,$$

defined by the line source of strength m; and

$$\bar{\boldsymbol{\Omega}} = \bar{\Omega}\mathbf{e}_\Phi$$

for the unperturbed vortex ring, which gives

$$\frac{D\boldsymbol{\Omega}'}{Dt} = \left(\frac{\bar{\Omega}}{\sigma}\frac{\partial}{\partial\Phi}\right)\mathbf{u}' + \boldsymbol{\Omega}'.\nabla\frac{m}{\sigma}\mathbf{e}_\sigma$$

and therefore

$$\frac{D\boldsymbol{\Omega}'}{Dt} = \frac{\bar{\Omega}}{\sigma}\frac{\partial\mathbf{u}'}{\partial\Phi} - \frac{\Omega'_\sigma m}{\sigma^2}\mathbf{e}_\sigma + \frac{\Omega'_\Phi m}{\sigma^2}\mathbf{e}_\Phi. \tag{14}$$

For an initially radial perturbation of the ring, the equation for the radial component of vorticity is, from (14),

$$\frac{D\Omega'_\sigma}{Dt} = -\frac{\Omega'_\sigma m}{\sigma^2},$$

which leads to

$$\Omega'_\sigma = E\exp\left[-mt/\sigma^2\right] + F, \tag{15}$$

where E, F are constant. From (15) we see that, for a source flow ($m > 0$), Ω'_σ is decreasing exponentially, and, for a sink flow ($m < 0$), Ω'_σ grows exponentially. Thus in the contracting element any small perturbation in the ring radius will cause an exponentially growing component of radial vorticity. This will cause axial deformations on the ring which could make major changes in the induced flow field. We might therefore conclude that expanding jet flows are stable to small perturbations whilst contracting jet flows are not.

This could then account for the discrepancy between our results and those of Lau *et al.* (1972); the entrained vortex ring elements contract, become unstable and non-axisymmetric and thus modify the induced flow field. Furthermore, the effect of the embeded slower moving fluid which Lau, Fisher & Fuchs suggest causes the negative spikes in the axial velocity traces can only be modelled in a vortex-sheet-type model by a 'kink' in the sheet. (This 'kink' causes vortex elements to be nearer the jet axis than the measuring station, and, whether stable or not, causes a decrease in axial velocity at

this measuring station.) However, consideration of our modelled flow (e.g. in figure 1*c* at $X/D \simeq 2{\cdot}2$) shows that, because the sheet is digitized, we are not able to model exactly the sheet when it becomes very thin. The layer here is then inadequately represented by just a single relatively concentrated vortex, which must then be drawn into the larger neighbouring concentrated eddies. This means that in our model the large eddies are perhaps more concentrated than in real jet flows and this explains why the r.m.s. levels of the axial and radial velocity fluctuations were larger than in real flows.

We have clearly shown that if individual eddying motions are to be studied, radial rather than axial velocity signals must be used, especially in the mixing region. We have shown this to be especially important when measuring eddy convection velocities from the velocity space–time correlations. The implication made when measuring velocity in this way, is that the 'phase' of exterior irrotational flow fluctuations moves at the speed of the eddies which cause them, i.e. the large eddies in the mixing region. As we have shown, this information is only contained in the radial velocity measurements. The measured values of the eddy convection velocities of the jet model show no apparent dependence on the forcing and approximately agree with the unforced jet measurement of $U_c/U_0 \simeq 0{\cdot}56$. This is much lower than the local mean velocity $\bar{U}/U_0 \simeq 0{\cdot}65$ (at $R/D = 0{\cdot}5$), which is in disagreement with many experimental results (e.g. Wills 1964) where the measured convection velocity is much closer to this local mean value. It does not seem likely that this discrepancy is caused by the velocity smoothing core, since this would then be expected to have the same effect on the mean local velocity. We have described the choice of the vortex core used to define the self-induced velocity which does fix some convection parameter of the flow, but we do not think that the discrepancy between the measured convection velocity and the local mean velocity is caused by a bad choice of core size. However, we can see that the calculated driving velocity (the convection velocity of a long cylindrical sheet composed of a single row of vortex rings, with the chosen core size) $U_d/U_0 \simeq 0{\cdot}54$ is close to the measured eddy convection velocity. This is not surprising since we would not expect the shear layer to travel faster just because eddies have formed. It is possible that the effects of non-axisymmetry may also be important in real jets in the measurements for the correlation coefficients.

We have attempted to model the axisymmetric jet in order to investigate the effect of forcing on the large eddy motion in the mixing region and to interpret the experimentally observed behaviour of forced jets. At forcing levels higher than 0·02 % of the jet exit velocity (Moore 1977) the observed response of the jet was nonlinear. It was then that the changes in broadband noise were observed, and the dramatic changes in eddy structure occurred. In our model jets, we have levels of forcing much higher than this. At $A = 0{\cdot}005$ ($\tilde{u}/U_e \simeq 0{\cdot}35\,\%$) there was little response to the forcing; our inadequate modelling of the effects of the jet pipe has meant that our required forcing levels are higher than those used in experiments.

In his experiments, Chan (1974) forced a turbulent jet in the frequency range $0{\cdot}2 \leqslant St \leqslant 0{\cdot}8$; the measured response to forcing grew rapidly then decayed downstream. At the higher Strouhal numbers the disturbances were confined to the first part of the mixing region, whilst at low Strouhal numbers the disturbance extended much further downstream. We can interpret this in terms of our results, where at high frequencies the eddies form more rapidly than at low frequencies and soon coalesce

and generate the subharmonic (the signal filtered at the forcing frequency would therefore decay). Chan also found that for high frequencies the centre-line signals are weaker than at low frequencies, which can also be interpreted in terms of the size of eddy generated. The disturbance most amplified was at $St = 0{\cdot}5$ for the shear layer, and at $St = 0{\cdot}35$ on the jet centre-line. This latter measurement agrees with the measurements of Crow & Champagne who forced the jet at $St = 0{\cdot}3$ and suggested that this is the wave least capable of generating a subharmonic and therefore the wave most capable of reaching a large amplitude before saturating. This is demonstrated in our model as the largest eddy forms further downstream when $St = 0{\cdot}3$ than when $St = 0{\cdot}5$, and it is bigger than the eddy which forms immediately downstream of the nozzle when $St = 0{\cdot}5$.

Thus we suggest that the nonlinear saturation occurs once the eddy structure is formed, and the filtered response decays once this eddy loses its identity. The results of Moore (1977) suggest that the broadband noise increase (at $St \simeq 0{\cdot}5$), and the decrease (at $St > 1{\cdot}5$) are associated with these changes in eddy structure. The natural periodicity of the model jet was $St \simeq 0{\cdot}47$, and when forced at approximately this frequency, the jet was most sensitive. Much larger eddies formed earlier here than in the jets forced at higher frequencies. The jet development was also more ordered in the resulting absence of coalescence. Our study of the coalescence process (Acton 1976) suggested that it was an abrupt large-scale and therefore noisy event and it seems clear the reduction of the size of the eddies makes the pairings much less violent. In fact, at $St = 0{\cdot}5$ we have seen from further computation (not shown) that a coalescence is about to occur at $X/D = 4{\cdot}0$ which would be a much larger motion and possibly a more regularly occurring event than that observed in the jets excited at high frequencies. The eddies which form when the jet is forced at high frequencies are much smaller than in the unforced jet and several smaller-scale interactions take place, resulting in a less regular, less well correlated eddy structure and thus might be associated with the observed decreases in broadband noise.

6. Conclusions

We have attempted to model numerically some features of turbulent jet flows. The model is axisymmetric, inviscid and restricted to the large-scale motions. The model jet shows many of the features observed in real jet flows. Discrepancies that do exist between our model results and those observed experimentally occur because the nozzle boundary conditions are not exactly satisfied and the flow is axisymmetric. We have shown that the contracting elements of jet vorticity are unstable and therefore axisymmetry is likely to be lost on the inside of the real jet mixing region.

We have applied harmonic excitation to the model jet. This changes the size and position of the first eddies that form and thus changes the location and frequency of any coalescence of the eddies. We have been able to show for these forced model jet flows that, in the Strouhal number range $0{\cdot}3 \leqslant St \leqslant 2{\cdot}0$, a forcing of sufficient amplitude could excite jet eddies at the forcing wavelengths. When $St = 0{\cdot}3$, these eddies were very large and formed after pairings, at $X/D \simeq 2{\cdot}0$. When the jet was forced at $St = 0{\cdot}5$, at highest amplitude of forcing the large eddies formed at $X/D \simeq 1{\cdot}0$ and persisted for several diameters downstream. At higher frequencies, these eddies which formed at the forcing frequency were small and quickly lost their identities by coalescence. This occurred nearer the jet-pipe exit when the amplitude was increased.

This behaviour is qualitatively consistent with many features of the non-linear large eddy behaviour observed in forced jets.

The good qualitative agreeement that does exist between our model and experimentally observed jet flows leads us to conclude that these flows have significant large-scale axisymmetric structure of the type we model.

This work is part of the research programme sponsored at Cambridge University by Rolls-Royce Ltd. The help and encouragement of Professor J. E. Ffowcs Williams is gratefully acknowledged. The author also wishes to thank the Director of Computing Service for use of the facilities of the University Computer.

REFERENCES

ACTON, E. 1976 The modelling of large eddies in a two-dimensional shear layer. *J. Fluid Mech.* **76**, 561–592.

BATCHELOR, G. K. 1970 *An Introduction to Fluid Dynamics*. Cambridge University Press.

BATCHELOR, G. K. & GILL, A. E. 1962 Analysis of the stability of axisymmetric jets. *J. Fluid Mech.* **14**, 529–551.

BECHERT, D. & PFIZENMAIER, E. 1975 On the amplification of broad band jet noise by a pure tone excitation. *J. Sound Vib.* **43**, 581–587.

BRADSHAW, P., FERRISS, D. H. & JOHNSON, R. F. 1964 Turbulence in the noise-producing region of a circular jet. *J. Fluid Mech.* **19**, 591–624.

BROWN, G. L. & ROSHKO, A. 1974 On the density effects and large structure in turbulent mixing layers. *J. Fluid Mech.* **64**, 775–816.

CHAN, Y. Y. 1974 Spatial waves in turbulent jets. *Phys. Fluids* **17**, 46–53.

CROW, S. C. & CHAMPAGNE, F. H. 1971 Orderly structure in jet turbulence. *J. Fluid Mech.* **48**, 547–591.

DAVIES, P. O. A. L., FISHER, M. J. & BARRATT, M. J. 1963 The characteristics of the turbulence in the mixing region of a round jet. *J. Fluid Mech.* **15**, 337–367.

DAVIES, P. O. A. L. & HARDIN, J. C. 1973 Potential flow modelling of unsteady flow. *Int. Conf. on Numerical Methods in Fluid Dynamics*, Dept. of Civil Engng, University of Southampton.

DIMOTAKIS, P. E. & BROWN, G. L. 1975 Large structure dynamics and entrainment in the mixing layer at high Reynolds number. *California Institute of Technology, Rep.* CIT-7-PU.

FISHER, M. J. & DAVIES, P. O. A. L. 1964 Correlation measurements in a non-frozen pattern of turbulence. *J. Fluid Mech.* **18**, 97–116.

KO, N. W. M. & DAVIES, P. O. A. L. 1971 The near field within the potential core of subsonic cold jets. *J. Fluid Mech.* **50**, 49–78.

LAMB, H. 1924 *Hydrodynamics*. Cambridge University Press.

LAU, J. C., FISHER, M. J. & FUCHS, H. V. 1972 The intrinsic structure of turbulent jets. *J. Sound Vib.* **22**, 379–406.

LAU, J. C. & FISHER, M. J. 1975 The vortex street structure of turbulent jets. Part 1. *J. Fluid Mech.* **67**, 229–338.

LEVINE, H. & SCHWINGER, J. 1948 On the radiation of sound from an unflanged circular pipe. *Phys. Rev.* **73**, 383–406.

MOORE, C. J. 1974 Aerodynamic data and flow visualisation techniques for the A.R.L. jet rig. *Rolls-Royce* (1971) *Ltd, Rep.* RR(OH)585.

MOORE, C. J. 1977 The role of shear layer instability waves in jet exhaust noise. *J. Fluid Mech.* **80**, 321–367.

SAFFMAN, P. G. 1970 The velocity of viscous vortex rings. *Stud. Appl. Math.* **49**, 371–380.

TOWNSEND, A. A. 1976 *The Structure of Turbulent Shear Flow*, 2 edn. Cambridge University Press.

WILLS, J. A. B. 1964 On convection velocities in turbulent shear flows. *J. Fluid Mech.* **20**, 417–432.